Seismic design and analysis of precast concrete buckling-restrained braced frames

Shane Oh, Yahya C. Kurama, Jon Mohle, and Brandt W. Saxey

- The study described in this paper investigated the lateral load behavior and design of precast concrete buckling-restrained braced frames and the feasibility of their use in seismic regions.

- Thirty-two precast concrete braced-frame archetypes were designed, and nonlinear numerical models of the structures were developed.

- Nonlinear static pushover analyses and incremental dynamic time-history response analyses were performed, and the analysis results were used to evaluate the seismic performance of the archetypes.

- This paper provides a recommended seismic design procedure and recommended seismic performance factors for precast concrete buckling-restrained braced frames and suggests topics for future research.

PCI Journal (ISSN 0887-9672) V. 66, No. 5, September–October 2021.

PCI Journal is published bimonthly by the Precast/Prestressed Concrete Institute, 8770 W. Bryn Mawr Ave., Suite 1150, Chicago, IL 60631.

Buckling-restrained braced frames are a type of lateral force-resisting system currently used primarily for steel buildings in moderate and high seismic zones. These structures resist lateral loads using buckling-restrained braces placed diagonally and connected to the beams and columns of the frame in each story. Although buckling-restrained braced frames are visually similar to conventional concentrically braced frames, the unique characteristics of buckling-restrained braces result in distinct behavior under seismic loads. Buckling-restrained braces are typically composed of a high-ductility steel core plate surrounded by a concrete- or grout-filled steel tube. Under compressive loads, the concrete- or grout-filled tube prevents buckling of the steel core plate (also known as the yielding core) to provide an axial strength of the brace in compression that is similar to the axial strength to the brace in tension. This characteristic creates stable and nearly symmetric hysteretic load-deformation behavior with large energy dissipation, allowing the yield strength of the steel core to dictate the design of the brace rather than the critical buckling load of the brace.[1–5]

Extensive research on steel buckling-restrained braced frames has demonstrated that properly designed and detailed frames concentrate damage during a seismic event in the yielding region of the braces, while the beams and columns essentially behave elastically.[3,6–9] These findings led to the codification of steel buckling-restrained braced frames for use in the United States beginning in the 2005 edition of the American Society of Civil Engineers' *Minimum Design Loads for Buildings and Other Structures* (ASCE 7-05),[10] with a larger response modification coefficient R of 8 compared with other braced-frame systems (for example, a response modification factor R of 6 for special concentrically braced frames). Consequently, buckling-restrained braced frames have become the lateral system of choice for many steel structures in seismic regions, where they are associated with significant reductions in costs as well as stable ductile lateral load behavior of the frame.

Despite the popularity of buckling-restrained braced frame systems in steel construction, they have rarely been used in concrete structures, in large part due to limited research and lack of codification. A few studies from outside the United States have investigated the use of buckling-restrained braces in reinforced concrete frames;[11–14] however, these studies have focused primarily on seismic retrofit applications rather than new construction. To the best of the authors' knowledge, no United States–based research on precast concrete buckling-restrained braced frames has been published, and only one experimental study (Guerrero et al.[15]) on the seismic behavior of these structures has been published worldwide. Consequently, practical implementation of precast concrete buckling-restrained braced frames has been rare, with limited applications in international projects and only one building application in the United States.[16]

In an effort to address this research gap, this paper numerically investigates the lateral load behavior and design of precast concrete buckling-restrained braced frames for potential feasibility in seismic regions. To this end, 32 precast concrete braced-frame archetypes were designed, and nonlinear numerical models of these structures were developed using the Open System for Earthquake Engineering Simulation (OpenSees)[17] structural analysis platform. The numerical model was validated using the results presented in Guerrero et al. and also by comparing the OpenSees analyses with the results obtained from a second structural analysis platform, DRAIN-2DX.[18] After the model was deemed suitable based on this validation, nonlinear static pushover analyses and incremental dynamic time-history response analyses were performed on the 32 archetypes. Ultimately, the analysis results were used to evaluate the seismic performance of the archetypes and the seismic performance factors used in their design.

To develop useful results grounded in a rational basis, this study followed many of the procedures described in the 2009 Federal Emergency Management Agency report *Quantification of Building Seismic Performance Factors* (FEMA P695),[19] which provides a methodology to formalize the determination of seismic performance factors (for example, the response modification coefficient) for new proposed lateral force-resisting systems. This methodology includes several steps to identify the range of application for the proposed system and accurately assess the seismic collapse risk. The first step is to develop and design a set of archetypes that span the range of expected applications, where an archetype is defined as a prototypical representation of the system. Second, nonlinear models are developed for each archetype. Third, these models are subjected to pushover analyses and incremental dynamic time-history response analyses as defined within the methodology. The dynamic analyses include the use of a prescribed ground-motion record set. Finally, the FEMA P695 methodology outlines a systematic evaluation of the analysis results based on the uncertainty and collapse performance of the system.

FEMA P695 requires extensive material, component, connection, and system testing for characterizing the behavior of the proposed system and for calibrating the analysis models. Because these extensive experimental data are not currently available for precast concrete buckling-restrained braced-frame structures, the study described in this paper is limited to the relatively small amount of experimental information available to date.

Overview of archetypes

This section describes the 32 precast concrete buckling-restrained braced-frame archetypes that were designed for evaluation based on the FEMA P695[19] methodology. Although all archetypes were designed with the same uniformly distributed gravity loads and material properties, various seismic design categories (SDCs), building plans, numbers of braced frames, brace configurations, and numbers of stories were considered to span the expected design space of the proposed structural system. Once established, these archetypes were then organized into performance groups in accordance with FEMA P695. The precast concrete beam and column members were designed using deformed steel reinforcement with no prestressing, considering details that emulate monolithic cast-in-place reinforced concrete structures. Jointed (also referred to as "nonemulative") precast concrete buckling-restrained braced-frame structures were not included in this study, but these types of precast concrete systems should be investigated in the future.

Archetype design space

Two SDCs were used for this study, SDC D_{max} and SDC D_{min}, as described by the spectral acceleration values provided in FEMA P695[19] Tables 5-1A and 5-1B. While the structures evaluated for SDC D_{max} were expected to be more critical, SDC D_{min} was also considered for a limited number of designs to capture any unexpectedly critical scenarios. To minimize structural overstrength and produce lower-bound designs, the archetypes designed for SDC D_{min} included fewer braced frames within their building plans.

Figure 1 shows the archetype space, which consisted of three different symmetric building footprints. All building plans had an area of about 30,000 ft^2 (2800 m^2). The first represented an office building with 15 ft (4.6 m) story heights, the second represented an industrial building with 25 ft (7.6 m) story heights, and the third represented an alternate industrial building layout with 15 ft story heights. The office building plan also included three different braced-frame layouts, which

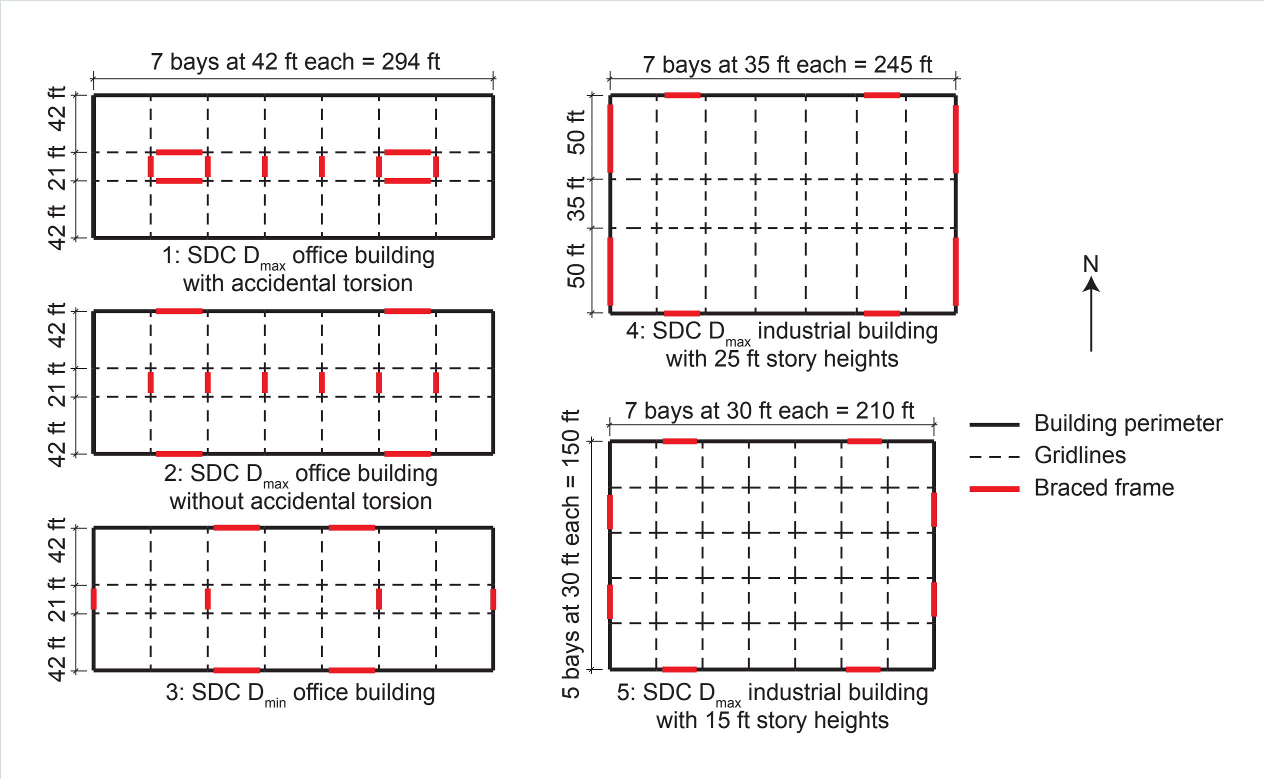

Figure 1. Building and braced-frame plan layouts. Note: SDC = seismic design category. 1 ft = 0.305 m.

considered different levels of accidental torsion effects and different numbers of braced frames. The first office layout was arranged with the braced frames placed toward the core of the building to introduce accidental torsion effects per the 2016 edition of *Minimum Design Loads and Associated Criteria for Buildings and Other Structures* (ASCE 7-16).[20] The second layout had the same number of braced frames in each direction, but accidental torsion effects were eliminated from design by placing the east-west braced frames along the perimeter of the building plan. The third layout was designed for SDC D_{min} using a significantly reduced number of braced frames arranged to eliminate accidental torsion effects. The industrial building layouts were both designed for SDC D_{max}, with braced frames at the exterior to eliminate accidental torsion effects. The building layouts without accidental torsion effects were expected to result in more critical FEMA P695 evaluations because these layouts were designed for lower seismic forces.

Three different buckling-restrained brace elevation configurations were investigated in this study: single diagonal, alternating single diagonal (also known as zigzag), and chevron. **Figure 2** presents these configurations within two-story frame archetypes. Given the large variety of possible arrangements, brace configurations deemed to be unlikely in precast concrete structures or less critical based on the FEMA P695 procedures were not included. For example, multistory X-bracing tends to be less critical because it minimizes the unbalanced vertical loading and axial loads transferred to the beams and distributes the brace yielding across multiple stories.[21] In contrast, single-diagonal braces result in high axial forces in the beams and chevron braces generate high bending moments in the beams. Therefore, these brace configurations were evaluated to capture the most critical conditions in the FEMA P695 methodology. The brace angle was also considered an important parameter in the design space; specifically, the different frame span lengths and story heights resulted in archetypes with brace angles ranging from 35.5 to 45.0 degrees from horizontal.

The range of archetypes used in the study included one-, two-, three-, four-, six-, and nine-story frames, with building

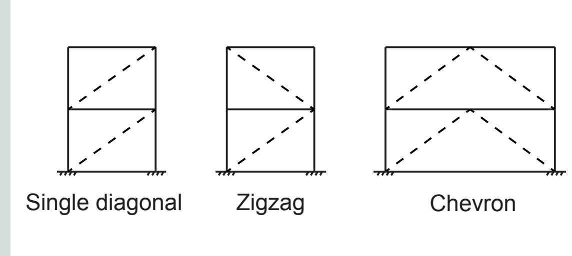

Figure 2. Brace configurations for two-story frame archetypes.

heights ranging from 15 to 135 ft (4.6 to 41.1 m). Based on preliminary results, archetypes taller than nine stories (taller than 135 ft) were less critical in the FEMA P695 methodology and were also deemed less likely to be implemented in precast concrete practice. Therefore, no archetypes taller than nine stories were included.

In the remainder of this paper, each archetype is labeled with a four character identifier, where the first character is the layout number (see Fig. 1), the next two characters indicate the brace configuration (see Fig. 2), and the last character is the number of stories. For example, archetype 1SD3 is a 3 story frame with single-diagonal braces in building plan layout 1.

Gravity loads

All archetypes were designed using the average distributed dead loads D and live loads L listed in **Table 1**. The total average roof and floor dead loads were taken as 160 lb/ft^2 (7660 N/m^2), including a precast concrete double-tee-beam flooring system with a 4 in. (100 mm) thick cast-in-place topping. The roof and floor average live loads were taken as 20 and 100 lb/ft^2 (960 and 4790 N/m^2), respectively.

Design material properties

For the design of all archetypes, the yield strength of the brace steel core was assumed to have the typical range of 42 ± 4 ksi (290 ± 28 MPa), corresponding to minimum yield strength f_{ymin} of 38 ksi (262 MPa), and maximum yield strength f_{ymax} of 46 ksi (317 MPa), respectively, based on section 5.5 of the American Institute of Steel Construction's (AISC's) third edition of the *Seismic Design Manual*[22] and common industry practice. The design yield strength of deformed reinforcing steel f_{sy} was 80 ksi (552 MPa) and the design compressive strength of concrete f'_c was 6 ksi (41.4 MPa). Given the large design axial tension forces in the beams and columns, the use of Grade 80 (552 MPa) rather than Grade 60 (414 MPa) reinforcing bars was necessary to minimize the sizes of these members while satisfying design requirements for maximum reinforcement ratios (see the "Design of Archetypes" section in this paper).

Table 1. Assumed overall average gravity loads

Dead loads	
Contribution	Average load per roof/floor area, lb/ft^2
Double-tee flooring	50
Topping slab	45
Beams and columns	25
Spandrels/exterior cladding	15
Partition loads	15
Buckling-restrained braces	5
Miscellaneous	5
Total dead load	160
Live loads	
Location	Average load per roof/floor area, lb/ft^2
Roof	20
Floor	100

Note: 1 lb/ft^2 = 47.9 N/m^2.

Performance groups

Table 2 shows the archetype designs grouped into nine performance groups for system evaluation per FEMA P695.[19] The frame designs within each performance group shared similar characteristics expected to influence the results of the seismic evaluation. For this study, the performance groups were determined based on brace configuration, seismic design category, and fundamental building period domain (short or long). FEMA P695 typically requires at least three archetypes for each performance group, though groups with fewer than three archetypes are allowed if having three or more alternate designs within a performance group is not considered feasible.

Design of archetypes

This section describes the procedures used to design the archetype braced-frame structures used in the investigation. The design method was based on the equivalent lateral force procedure from ASCE 7-16[20] and followed the American Concrete Institute's *Building Code Requirements for Structural Concrete (ACI 318-19) and Commentary (ACI 318R-19)*[23] for the design of the precast concrete beams and columns. Several applicable design requirements and recommendations for steel buckling-restrained braced frames were also adopted, particularly with respect to the design of the braces and the resulting design forces on the beams and columns, referencing AISC's *Seismic Design Manual*,[22] Specification for Structural Steel Buildings (ANSI/AISC 360-16),[24] and *Seismic Provisions for Structural Steel Buildings* (ANSI/AISC 341-16),[25] as well as the Structural Engineers Association of California's (SEAOC's) *Structural/Seismic Design Manual*.[26]

Based on preliminary designs, trial values of the required seismic performance factors were chosen as follows: response modification coefficient R of 8, deflection amplification factor C_d of 8, and system overstrength factor Ω_0 of 2.5. These values were then verified in the final step of the FEMA P695[19] evaluation. The selected response modification coefficient R and system overstrength factor Ω_0 values are the same as those for steel buckling-restrained braced frames, but the deflection amplification factor C_d of 8 is greater than the value of 5 specified for steel buckling-restrained braced frames in ASCE 7-16.

Table 2. Performance group summary

Performance group number	Grouping criteria				Number of archetypes
	Brace configuration	Design load level		Period domain	
		Gravity	Seismic design category		
1	Single diagonal (with torsion)	Typical	D_{max}	Short	3 (1, 2, and 3 stories)
2	Single diagonal		D_{max}	Short	5 (1, 2, and 3 stories)
3				Long	4 (6 and 9 stories)
4			D_{min}	Short	3 (1, 2, and 3 stories)
5	Chevron		D_{max}	Short	5 (1, 2, and 3 stories)
6				Long	3 (4, 6, and 9 stories)
7			D_{min}	Short	3 (1, 2, and 3 stories)
8	Zigzag		D_{max}	Short	3 (1, 2, and 3 stories)
9				Long	3 (4, 6, and 9 stories)

Figure 3 presents a summary flowchart of the design procedure; subsequent sections of this paper describe each component of the flowchart. The design procedure focuses on the lateral force-resisting braced frames, not the entire building structure. Consequently, detailed design of the gravity load system was not conducted. Furthermore, because this study evaluated the overall behavior of the braced-frame system, the brace-to-frame connections are not addressed. To this end, it is implicitly assumed that the brace-to-beam and brace-to-column connections would be designed to remain essentially linear-elastic under the maximum brace forces, following capacity-based design procedures.

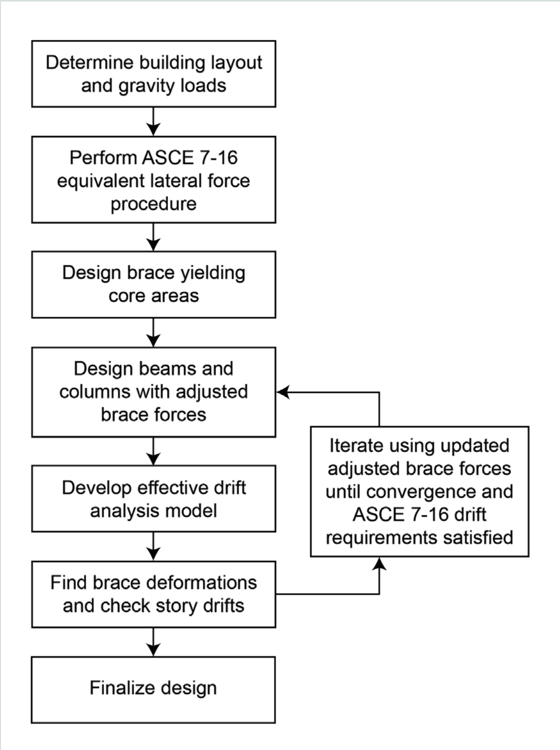

Figure 3. Archetype design flowchart.

Equivalent lateral force procedure

The ASCE 7-16[20] equivalent lateral force procedure was used to determine the lateral forces for the design of the archetype frames. **Table 3** shows the short-period design spectral acceleration parameter S_{DS} and 1-second design spectral acceleration parameter S_{D1}, taken for SDC D_{max} and SDC D_{min}, per FEMA P695.[19]

FEMA P695 defines the fundamental period T used for design and analysis as

$$T = C_u T_a$$

Table 3. Design spectral acceleration parameters

Seismic design category	S_{DS}	S_{D1}
D_{max}	1.0	0.60
D_{min}	0.50	0.20

Note: S_{D1} = design spectral response acceleration parameter at 1-second period; S_{DS} = design spectral response acceleration parameter at short periods.

where

C_u = coefficient for upper limit on the calculated period from ASCE 7-16 Table 12.8-1

T_a = approximate fundamental period from ASCE 7-16 section 12.8.2.1

Assuming comparable vibration characteristics, the approximate fundamental period T_a was calculated using the coefficients specified for steel buckling-restrained braced frames in ASCE 7-16 Table 12.8-2. Based on the design spectrum and this fundamental period, the total seismic base shear force V_{ELF} was determined using ASCE 7-16 Eq. (12.8-1), with the seismic response coefficient based on ASCE 7-16 section 12.8.1.1 and the seismic weight taken as 1.0D (which was assumed to be the same at each floor level, including the roof, as shown in Table 1) per ASCE 7-16 section 12.7.2. These calculations used a seismic importance factor I_e of 1 with Risk Category I or II, assuming that the office and industrial buildings included in the archetype space represented low risk to human life in the event of failure (ASCE 7-16 Table 1.5-1). This choice was made to result in more-critical archetypes for the FEMA P695 evaluation.

Next, the total seismic base shear force was distributed between the buckling-restrained braced frames in each of the two primary directions of the building. Because the braced frames in each direction were assumed to be the same, the lateral stiffnesses of these frames were also identical; and thus, the total seismic base shear was divided evenly between the frames in each direction. The base shear forces were increased as necessary to account for accidental torsion effects based on the procedures outlined in Paulay and Priestley,[27] assuming the sum of the frame stiffnesses in one direction to be equivalent to the sum of the frame stiffnesses in the orthogonal direction. As permitted by ASCE 7-16 section 12.8.4.2, the building plans with braced frames on the perimeter (layouts 2 through 5 in Fig. 1) resulted in designs without any accidental torsion effects. Once distributed to each individual frame, the base shear force was then distributed vertically over the height of the structure at each floor and roof level, per ASCE 7-16 section 12.8.3.

Brace design

The buckling-restrained braces were designed based on the brace axial forces N_{QE} from the ASCE 7-16[20] equivalent lateral force procedure and the expected yield strength of the yielding region of the braces. The brace forces in each story were calculated as

$$N_{QE} = V_{story}/[n_b \cos(\alpha)]$$

where

V_{story} = shear force in story being designed

α = angle of brace relative to horizontal

n_b = number of braces in the story being designed

This calculation for the brace axial force N_{QE} conservatively assumed that only the braces would carry lateral forces, with no contribution from beam and column moment frame action (similar to Design Example 3 from the SEAOC *Structural/Seismic Design Manual*[26] and section 5.5 of the AISC *Seismic Design Manual*[22] for steel buckling-restrained braced frames). The brace axial force N_{QE} values were then increased to account for second-order effects using the approximation provided in ANSI/AISC 360-16[24] appendix 8. Finally, the factored brace design axial force N_u was calculated based on ASCE 7-16 load combinations. Per AISC 341-16[25] section F4.3, the braces were assumed not to carry any gravity loads to ensure that the beam and column members of the frame were designed for the full gravity loads in the event of loss of braces (for example, due to fire loading). As such, the factored brace design forces under load combinations 6 and 7 were calculated as

$$N_u = \varrho N_{QE}$$

where

ϱ = redundancy factor, taken as 1.0 based on ASCE 7-16 section 12.3.4

Next, the yielding core areas of the braces were calculated using the area-based approach described in the AISC *Seismic Design Manual*. With this approach, the required brace core area was determined based on the lowest expected steel yield strength f_{ymin}. Thus, including a capacity reduction factor ϕ of 0.9, the minimum required steel core area of each brace was calculated as

$$A_{sc,min} = N_u/(\phi f_{ymin})$$

The resulting ranges of brace yielding (core) areas and yielding lengths over the height of each archetype design are listed in **Table 4**, where the required areas have been rounded up to the next 0.10 in.^{2} (64.5 mm^2) increment to achieve realistic designs with minimal overstrength.

After the yielding area of each brace was designed, the adjusted brace forces were determined based on the highest expected steel core yield strength f_{ymax} for use in the design of the beams and columns, following a capacity-based design approach. The adjusted brace forces were calculated according to ANSI/AISC 341-16 section F4.2a as

$$BRB_T = \omega R_y f_{ymax} A_{sc}$$

$$BRB_C = \beta \omega R_y f_{ymax} A_{sc}$$

where

Table 4. List of archetypes with corresponding range of brace yielding (core) areas and brace yielding lengths

Performance group	Archetype design identification number	Design configuration		Range of brace yielding areas, in.^{2}	Range of brace yielding lengths, in.
		Number of stories	Seismic design category		
1	1SD1	1	D_{max}	4.9	197
	1SD2	2		6.5 to 9.9	170 to 188
	1SD3	3		6.2 to 12.2	164 to 198
2	2SD1	1	D_{max}	3.8	186
	2SD2	2		5.1 to 7.6	186 to 192
	2SD3	3		4.8 to 9.4	182 to 193
	4SD1	1		6.1	382
	4SD2	2		6.3 to 9.2	336 to 395
3	1SD6	6	D_{max}	4.7 to 14.7	158 to 190
	1SD9	9		4.0 to 16.6	129 to 198
	2SD6	6		3.6 to 11.3	176 to 201
	2SD9	9		3.1 to 12.6	154 to 215
4	3SD1	1	D_{min}	2.9	197
	3SD2	2		2.7 to 4.0	195 to 197
	3SD3	3		2.3 to 4.6	193 to 198
5	2CC1	1	D_{max}	2.9	202
	2CC2	2		3.8 to 5.9	191 to 199
	2CC3	3		3.6 to 7.1	186 to 199
	5CC1	1		3.3	311
	5CC2	2		3.5 to 5.0	302 to 310
6	2CC4	4	D_{max}	3.2 to 3.7	184 to 201
	2CC6	6		2.7 to 8.5	178 to 202
	2CC9	9		2.3 to 9.6	163 to 196
7	3CC1	1	D_{min}	1.5	208
	3CC2	2		1.4 to 2.0	206 to 208
	3CC3	3		1.2 to 2.3	205 to 209
8	2ZZ2	2	D_{max}	5.1 to 7.6	186 to 192
	2ZZ3	3		4.8 to 9.4	182 to 193
	4ZZ2	2		6.3 to 9.2	336 to 395
9	2ZZ4	4	D_{max}	4.3 to 10.1	180 to 194
	2ZZ6	6		3.6 to 11.3	178 to 196
	2ZZ9	9		3.1 to 12.5	155 to 215

Note: CC = chevron brace configuration; SD = single-diagonal brace configuration; ZZ = zigzag brace configuration. 1 in. = 25.4 mm; 1 in.^{2} = 645 mm^2.

BRB_T = brace force in tension

β = adjustment factor for brace force in compression

ω = strain-hardening adjustment factor

R_y = expected yield-strength adjustment factor accounting for material variability

A_{sc} = area of the steel core

BRB_C = brace force in compression

For preliminary design, the compression force adjustment factor β was assumed as 1.1 and the strain-hardening adjustment factor ω was assumed as 1.4. Because material variability was already accounted for by designing the brace areas based on the minimum yield strength f_{ymin}, while using the maximum yield strength f_{ymax} for the adjusted brace forces (used to design the rest of the frame), the expected brace yield strength adjustment factor R_y was equal to 1 in all of the adjusted brace force calculations.

The design flowchart in Fig. 3 shows that the adjusted brace forces were revised based on the brace deformations determined from an effective linear-elastic analysis of the preliminary frame design, which is described later in this paper. Once the effective linear drift analysis of each preliminary archetype was completed, the adjusted brace forces and resulting frame designs were iterated using updated values for the compression force adjustment factor β and strain-hardening adjustment factor ω.

Beam design

The precast concrete beams of each archetype were designed based on the factored axial force P_u and bending moment M_u demands from ASCE 7-16[20] load combinations and the adjusted brace forces in tension BRB_T and compression BRB_C. Unlike traditional beam design, the large compressive and tensile axial forces of the buckling-restrained braces required the beams to carry large axial forces from earthquake effects in addition to moments and shear forces from gravity loads. Therefore, the beams were assumed to act like column members, and the design of the beams followed the column requirements for special moment frames in ACI 318[23] chapter 18, rather than the equivalent requirements for beams.

Because gravity loads do not produce axial forces in beams, the factored design axial force P_u in each beam was calculated from load combinations 6 and 7 based solely on the adjusted brace forces, following the requirements of ANSI/AISC 341-16[25] section F4.3. The exact relationship between the beam axial forces and the adjusted brace forces depends on the seismic load path, tributary mass, collectors on either side of the frame, and the distribution of forces throughout the entire structure. For simplicity, however, several assumptions for each brace configuration guided the relationship between the adjusted brace forces and the beam design axial forces in this study, as described in the following paragraphs.

For the single-diagonal brace configuration, the beam design axial forces were calculated using the adjusted brace forces directly above and below the beam being designed. Assuming that the earthquake-induced shear force in the building could be evenly transferred from both ends of the frame, the axial force in each beam was calculated as the average horizontal component of the two adjusted brace forces. In this calculation, the beam tensile axial force demand corresponded to the direction of lateral loading with the braces in compression, whereas the beam compressive axial force demand corresponded to the loading direction with the braces in tension.

A similar procedure was followed for the beam design axial forces with braces in the zigzag configuration, using the adjusted brace forces directly above and below the beam. However, in this configuration, one brace will be in tension while the other is in compression. Therefore, the beam axial force demands were calculated conservatively as the difference between the horizontal components of the absolute adjusted brace forces directly above and below the beam. The axial forces were calculated considering lateral forces acting to the left and the right, and the largest compressive and tensile forces from either direction were used as the axial force demands on each beam.

For the chevron brace configuration, the beam design axial force demands were calculated based on the two buckling-restrained braces below the beam in consideration. This configuration results in a large horizontal force at the connection between the buckling-restrained braces and the midlength of the beam because one of the braces will be in tension while the other is in compression. This force is carried as tension in half of the beam length and compression in the other half, though the exact distribution of this force between the two halves of the beam depends on the load path. In addition, each half length of a beam can experience tension as well as compression, depending on the direction of loading. In this study, the two halves of each beam were assumed, for simplicity, to have an even tributary area, thus evenly carrying the horizontal force from the braces. Therefore, each beam was designed for tensile and compressive axial forces equal to one-half of the sum of the horizontal components of the adjusted brace forces.

The factored design bending moment demands M_u for the beams were determined from both gravity loads and earthquake effects. Although Table 1 lists the average distributed dead and live loads assumed for the entire structure, some of the dead loads were not carried by the beams. Therefore, all beams were designed for a smaller dead load of 130 lb/ft^2 (6220 N/m^2) to exclude the weight of the buckling-restrained braces, columns, and exterior cladding. For beams at the exterior (that is, perimeter) of the structure, an additional vertically distributed 35 lb/ft^2 (1700 N/m^2) dead load was included to account for the exterior cladding weight. The live loads listed in Table 1, reduced per ASCE 7-16 section 4.7, were used for the beam design.

The gravity moments were then calculated based on the factored dead and live loads over the tributary width of each beam, and the orientation of the double-tee flooring system. For the archetypes with single-diagonal and zigzag brace configurations, the flooring system was assumed to run perpendicular to the beam on both sides (that is, the floor and roof double tees were assumed to be framing into the beams), thus transferring dead and live loads onto the beams. For the chevron brace configuration, the double tees were assumed to run parallel to the frame. Therefore, each beam was only designed for dead and live loads from the beam self-weight, weight of topping slab directly above the beam width, exterior cladding on perimeter beams, and live load directly above the beam width. These different assumptions for the orientation of the flooring system were made to evaluate effects of gravity load variations on the design and performance of the beams.

Different boundary conditions were considered to determine the largest positive and negative beam bending moment demands. For gravity loads, the maximum negative moments at the beam ends were calculated assuming fixed end supports, while the maximum positive moment at the midlength was calculated assuming simply supported boundary conditions (similar to section 5.5 of the AISC *Seismic Design Manual*[22] for steel buckling-restrained braced frames). For braces in the chevron configuration, an additional negative beam moment due to gravity loads was calculated at the brace location (that is, midlength of beam) assuming a simply supported two-span continuous beam (similar to Design Example 3 in the SEAOC *Structural/Seismic Design Manual*[26]).

For the chevron brace configuration, beam bending moments also develop from earthquake effects because the brace forces directly below the beam, one in compression and the other in tension, generate a net upward point load F_y of $\left(\left|BRB_C\right|-\left|BRB_T\right|\right)sin(\alpha)$ at the beam midlength (section 5.5 in the AISC *Seismic Design Manual* and Design Example 3 from the SEAOC *Structural/Seismic Design Manual*). The moments caused by this point load were calculated assuming a simply supported beam with the net upward point load F_y acting at the midlength and used in load combinations 2, 6, and 7 to find the total factored design moments for each beam. For frames with single-diagonal and zigzag brace configurations, the braces were assumed to be pin connected at the beam-to-column joints such that the brace forces resulted in no significant bending moments on the beams.

The beams were designed for the combined factored axial force P_u and bending moment M_u demands for each load combination. Because each beam was designed based on the requirements for columns in special moment frames in ACI 318 chapter 18, the longitudinal reinforcement ratio was kept between 1% and 6% (ACI 318 section 18.7.4.1). The large axial tensile forces and the maximum reinforcement limit of 6% tended to generate excessively large member sizes when using Grade 60 (414 MPa) reinforcement. Therefore, Grade 80 (552 MPa) reinforcing steel was used consistently instead. For simplicity, all beams were designed as rectangular sections with a 4 in. (100 mm) thick cast-in-place topping slab placed to act compositely on top of the beam (**Fig. 4**). For configurations with the floor and roof double tees oriented perpendicular to the braced frame, the beams were designed as T beam sections with an effective topping slab flange width per ACI 318 Table 6.3.2.1 and eight no. 6 (19M) reinforcing bars assumed within this topping slab width. For configurations with the floor and roof system running parallel to the braced frame, the effective width of the topping slab was limited to the width of the beam, with only two no. 6 reinforcing bars assumed within this slab width (Fig. 4). Because a full design of the floor and roof system was not conducted, the number and size of the topping slab reinforcing bars were selected based on typical industry designs.

The beams were designed for each factored axial-moment (P_u-M_u) load combination pair using interaction diagrams generated in MATLAB. **Fig. 5** shows a representative beam interaction diagram. The interaction diagrams considered both positive and negative bending, as well as compressive and ten-

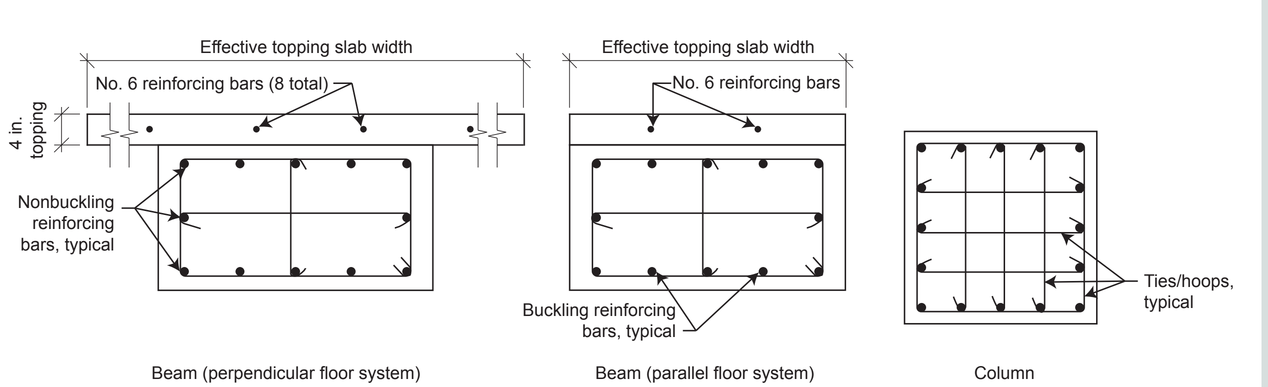

Figure 4. Sample beam and column cross sections in braced-frame archetypes. Note: no. 6 = 19M; 1 in. = 25.4 mm.

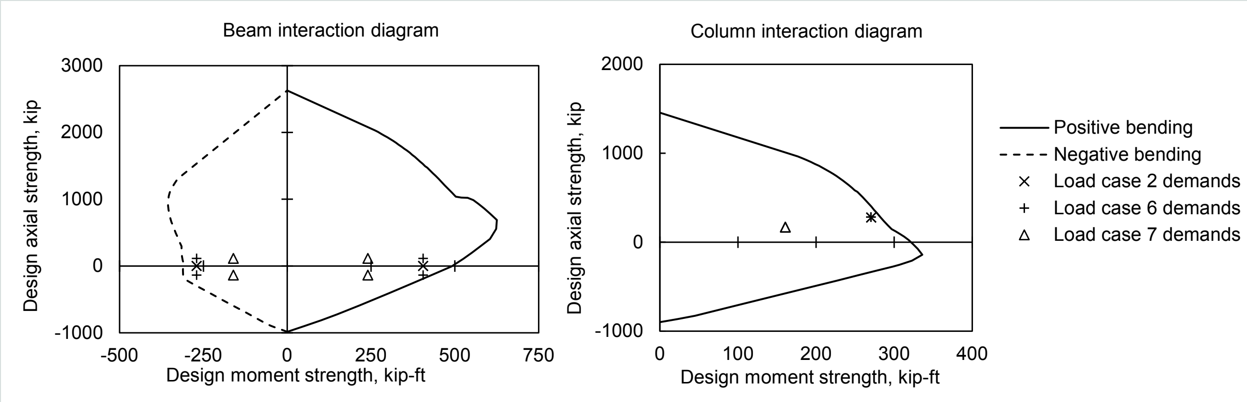

Figure 5. Sample axial-moment strength interaction diagrams for beam and column design. Note: 1 kip = 4.45 kN; 1 kip-ft = 1.356 kN-m.

sile axial forces, and the contribution of the assumed effective topping slab width and reinforcement to the axial-moment strength was included. In generating the interaction diagrams for design, the stress-strain behavior of the reinforcement was idealized as elastic, perfectly plastic. The design of each beam was considered to be satisfied if all applicable load combination pairs fell within the interaction diagram with minimal overstrength so as to result in critical archetypes for the FEMA P695[19] evaluation.

Finally, the design of each beam was checked for shear requirements. Although a full shear reinforcement design was not performed, the ACI 318 section 22.5.1.2 limits for the maximum allowable shear strength based on material strengths and the dimensions of each member were checked. The corresponding beam shear force demands were calculated based on ACI 318 Fig. 18.6.5 to ensure that the maximum allowable shear strength was not exceeded. Per ACI 318 section 18.7.6.1.1, the shear demand was checked against the strength over the range of the factored design axial forces. The shear design requirements often governed the beam dimensions, resulting in beam widths greater than the corresponding beam depths to satisfy shear demands without significantly increasing the beam moment strengths.

Column design

The columns were designed for the combined factored axial force P_u and bending moment M_u demands from ASCE 7-16[20] load combinations 2, 6, and 7. The axial force demands due to gravity loads were calculated by multiplying the factored dead and live loads by the tributary area for each column. Earthquake effects caused both axial compressive and tensile force demands in the columns, considering equivalent lateral forces in each direction of the frame. These demands were calculated using the vertical components of the adjusted brace forces in all of the braces above the column being designed. For the chevron brace configuration, the net upward force F_y due to the unequal adjusted brace forces at the beam midlength was also considered by assuming that the columns at each end of the beam carried $0.5F_y$ as axial tension.

AISC 341-16[25] section F4.3 allows column bending moments from seismic effects to be neglected, assuming that the portion of story shear resisted by these moments is generally small (Kersting et al.[21]). As such, only the moment demands from gravity loads were used in column design. The procedure to calculate these moment demands was based on the SEAOC *Structural/Seismic Design Manual*,[26] where the beam end moments from gravity loads (assuming fixed-fixed beam end boundary conditions) are distributed to the connecting columns. This distribution assumes points of zero moment at the column base (above the foundation) and at the midheight of each upper story (in other words, each story except the first story) and constant shear force along the column height between those points.

Similar to the beams, the columns were designed using axial-moment strength interaction diagrams generated in MATLAB. Figure 5 shows a representative column interaction diagram. Because each column was symmetric, these interaction diagrams only considered positive bending moments. The column longitudinal reinforcement percentages were kept within the range of 1% to 6%, and Grade 80 reinforcement was used to minimize the column sizes. For simplicity, longitudinal reinforcing bars were only placed around the section perimeter, and the column reinforcing bars over each story height were designed to be the same size. Per typical precast concrete industry practices, the column dimensions were changed only every third story.

ACI 318[23] section 18.7.3.2 enforces strong column–weak beam behavior for special reinforced concrete frames by requiring that

$$\Sigma M_{nc} \geq (6/5)\Sigma M_{nb}$$

where

ΣM_{nc} = sum of nominal moment strengths of the columns framing into each joint

ΣM_{nb} = sum of nominal moment strengths of the beams framing into the same joint

This requirement was indirectly satisfied (that is, without specifically considering ACI 318 section 18.7.3.2) for most of the columns in each archetype structure; however, some of the column sections in the upper two or three stories of the taller archetypes did not satisfy this requirement. Because it was deemed important to design critical structures with minimal overstrength for the FEMA P695[19] evaluation, the column section sizes and/or reinforcement amounts were not increased to achieve $\Sigma M_{nc} \geq (6/5)\Sigma M_{nb}$.

Each column design was also checked to meet shear requirements. Similar to the beams, a full shear reinforcement design was not performed for the columns; however, the ACI 318 maximum shear force demands were calculated to ensure that the maximum allowable shear strength limits were not exceeded. Unlike beam design, shear requirements never governed the column dimensions.

Effective linear-elastic drift analysis model

After the preliminary design of all frame members was completed, an effective linear-elastic equivalent lateral force pushover analysis for each archetype was conducted to check that allowable story drift limits per ASCE 7-16[20] were satisfied. As described in the flowchart in Fig. 3, the brace deformations from this step were also used to iterate the adjusted brace forces (by updating the adjustment factor for brace force in compression β and strain hardening adjustment factor ω) and update the design of the beams and columns accordingly. To ensure accurate drift analysis results at the equivalent lateral force level, several effective stiffness parameters were used to represent each beam, column, and brace member linear elastically. Each brace was modeled as a single element connected at the frame work points, assumed to be at the intersecting centroids of the beam and column members (**Fig. 6**), with an area equal to the yielding area and a stiffness modification factor (greater than 1.0) to account for the added stiffness from the much stiffer end regions of the brace. These brace stiffness modification factors were recalculated after iteration, as necessary, ranging from stiffness increases of 35% to 90%, depending on the brace size and geometry. The ends of each brace were assumed to be pinned into each work point node, thus transferring only axial forces along the brace axis.

The beam and column members were modeled with the axial and flexural stiffness reduction factors shown in **Table 5** based on the gross area A_g and gross moment of inertia I_g of each member. These factors are based on ACI 318[23] Table 6.6.3.1.1(a) and Table 6.6.3.1.1(b), which provide area and moment of inertia reduction factors for effective linear-elastic analysis at factored load levels. However, some modifications were necessary because the ACI 318 effective stiffness factors do not account for the increased cracking and stiffness reduction expected to occur due to the large axial tension forces in the beams and columns of buckling-restrained braced frames. The recommended mod-

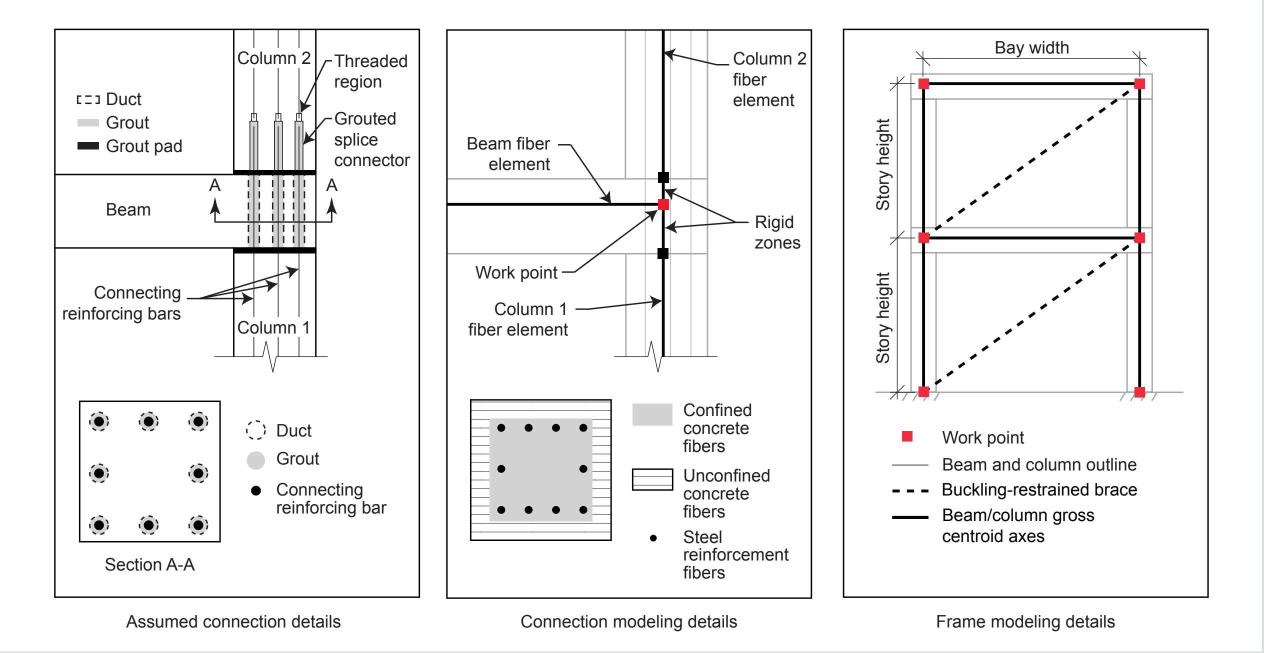

Figure 6. Illustration of beam-to-column connection region assumptions and frame modeling details.

Table 5. Effective area and moment of inertia reductions for beam and column members

Axial force	Area	Moment of inertia
Tension	$0.5A_g$	$0.25I_g$
Compression	$1.0A_g$	$\left(0.80+25\frac{A_{st}}{A_g}\right)\left(1-\frac{M_u}{P_u h}-0.5\frac{P_u}{P_o}\right)I_g$*

Note: A_g = gross area of beam or column section, neglecting reinforcement; A_{st} = total area of longitudinal reinforcement in beam or column section; h = depth of beam or column section; I_g = gross moment of inertia of beam or column section, neglecting reinforcement; M_u = factored design moment of beam or column; P_o = nominal compression (uniaxial) strength of beam or column at zero eccentricity; P_u = factored design axial force of beam or column (positive for compression and negative for tension).

*See the American Concrete Institute's *Building Code Requirements for Structural Concrete (ACI 318-19) and Commentary (ACI 318R-19)* Table 6.6.3.1.1(b); not to exceed $0.875I_g$ or be taken less than $0.35I_g$.

ification factors were calibrated to match the deformations of the effective linear-elastic drift model to a more detailed nonlinear inelastic model at the design equivalent lateral force level (see the next section of this paper, "Nonlinear Numerical Modeling").

Because the beam and column effective moment of inertia reduction factors for compression varied depending on the factored design axial force P_u and bending moment M_u, the effective drift calculations were conducted iteratively. The ASCE 7-16 requirements for drift calculations also resulted in the following additional steps in this iterative process:

1. Determine the fundamental period of the preliminary effective linear-elastic drift model from modal analysis.

2. Use this fundamental period to update the equivalent lateral forces. Because the period of the effective drift model was usually longer than the capped period used in the force-based member design, this step typically resulted in lower equivalent lateral forces for drift checks.

3. Perform a pushover analysis on the effective drift model under the updated equivalent lateral forces. This analysis included gravity loads based on the applicable ASCE 7-16 load combinations, and P-Δ effects were included per ASCE 7-16 section 12.8.7.

4. Determine the beam and column axial forces and bending moments from the effective drift analysis at the equivalent lateral force level.

5. Use these axial loads P_u and moments M_u to revise the moment of inertia reductions for members in compression per Table 5, and update the effective drift model accordingly.

By repeating this process until convergence, a different effective drift model was created for each ASCE 7-16 load combination, and the largest story drift values were taken as the governing values. Among load combinations 2, 6, and 7, load combination 7 typically governed the drift results.

After all governing effective linear-elastic story drifts θ_e were determined, the corresponding inelastic drifts θ were calculated using a proposed deflection amplification factor C_d of 8 for this system, as

$$\theta = C_d\theta_e$$

These inelastic drift θ values were then compared with the requirements of ASCE 7-16 Table 12.12-1, which prescribes a maximum allowable story drift of 2.5% for structures with four stories or fewer and 2% for all other structures. If the ASCE 7-16 drift limits were exceeded, all column cross-section dimensions over the entire structure height were scaled up until the drift requirements were met. No changes were made in the beam sizes because preliminary analysis results showed that the axial deformations of the columns typically controlled the drifts from the effective linear-elastic model. Using this approach, only the nine-story archetypes were drift controlled. All other archetypes were controlled by strength design.

Finally, the effective linear-elastic drift model results were used to iterate the brace designs. ANSI/AISC 341-16[25] section F4 requires buckling-restrained braces to be designed for deformations corresponding to a prescribed 2% story drift or twice the inelastic story drift (that is, 2θ), whichever is larger. The brace deformations were used to adjust the brace overstrength factors (adjustment factor for brace force in compression β and strain hardening adjustment factor ω) and the stiffness modification factors used in design.

Common practice in steel buckling-restrained brace design calculates equivalent brace deformations from story drifts using a simplified shear frame model, where the beam and column members are assumed to be axially rigid. Even though these assumptions may work reasonably well for steel frames, where the member stiffnesses are similar in tension and compression, significant axial elongations can occur in concrete beam and column members due to reduced effective axial stiffnesses from cracking. Specifically, the beams and columns of the archetype precast concrete buckling-restrained braced frames showed large axial elongations, thus contributing significantly to the effective story drifts. As such, each brace was designed for the larger of the following two deformations to avoid excessive overestimation of the brace deformations:

- deformations in the brace elements of the effective linear-elastic drift model at the equivalent lateral force level (corresponding to effective linear-elastic story drift θ_e) multiplied by the deflection amplification factor C_d

- equivalent brace deformations at 2% story drift based on shear frame assumptions (that is, assuming beam and column members are axially rigid)

In this approach, equivalent brace deformations calculated based on shear frame assumptions with twice the inelastic story drifts (that is, 2θ) from the effective drift model were deemed unreasonable for precast concrete frames and, therefore, were not used to design the braces. After calculating the brace deformations, the corresponding brace overstrength and stiffness modification factors were updated as needed in consultation with the brace manufacturer, and the iterative process was repeated. Once all brace factors converged and the ASCE 7-16 drift requirements were met, the design was considered complete.

Nonlinear numerical modeling

This section describes the detailed nonlinear numerical modeling and model validation of the precast concrete braced-frame system that was used in the FEMA P695[19] evaluation. The models were developed using the OpenSees[17] structural analysis platform.

Element and material models

Figure 6 shows the assumed arrangement for the connections between the beams and columns, with grouted vertical steel reinforcing bars connecting the precast concrete columns through the beams, leaving a precast concrete joint at the interface of each column connecting to the beam. Therefore, each beam was modeled from work point node to work point node, whereas the columns were modeled with rigid end zones within the beam-column joints. The work point nodes were assumed to be at the intersecting centroids of the beam and column members.

To account for nonlinear axial-flexural behavior, each beam and column member was modeled as a fiber element using two steel material models for the longitudinal (that is, axial-flexural) reinforcing bars and two material models for the concrete. **Figure 7** shows the stress-strain relationships for the reinforcing steel and typical unconfined concrete and brace materials.

The two reinforcing steel material models included a buckling reinforcing bar model and a nonbuckling reinforcing bar model. Both of these materials were modeled using the Steel4 uniaxial material type in OpenSees,[17] together with the MinMax material limit. Steel4 is based on the Giuffré-Menegotto-Pinto Steel02 material model, but it provides additional parameters to allow better simulation of the nonlinear cyclic steel stress-strain relationship. The MinMax material was applied to the Steel4 parent material, allowing simulation of steel rupture in tension and buckling in compression by reducing the steel stress to zero after a user-defined strain limit was exceeded. Both buckling and nonbuckling reinforcing bar materials were assumed to rupture at a tensile strain of 0.06, based on reversed-cyclic reinforcing bar test results by Aragon et al.[28] In addition, the buckling reinforcing bar material was assumed to buckle when the compression strain exceeded 0.004, which was the assumed crushing strain for the surrounding unconfined cover concrete, indicating possible loss of lateral support to the reinforcing bar from the concrete.

The following criteria were considered to determine which reinforcing bars would be modeled as buckling and which would be modeled as nonbuckling bars in each cross section. ACI 318[23] section 18.7.5 requires a transverse seismic hook or the corner of hoop reinforcement supporting every longitudinal reinforcing bar in a cross section when $P_u > 0.3A_g f_c'$. Because most of the beams and columns had large axial compression P_u demands, nearly all of the longitudinal reinforcing bars in each section were supported by seismic hooks or the corner of hoop reinforcement (Fig. 4). Previous studies (Brown and Kunnath,[29] Kunnath et al.,[30] and Mander et al.[31]) have shown that reinforcing bars are less likely to buckle if the

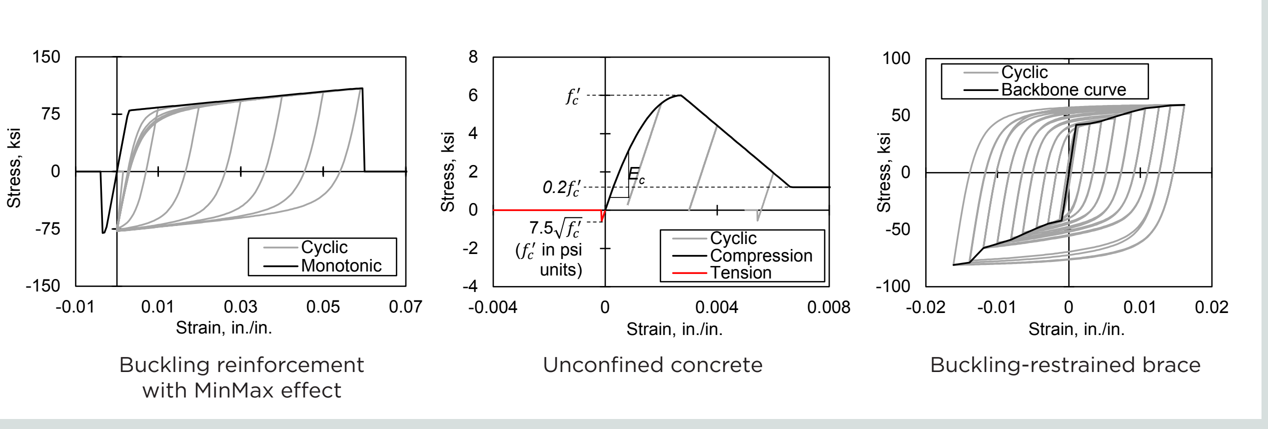

Figure 7. Buckling reinforcement stress-strain curves with MinMax effect, unconfined concrete stress-strain curve, and buckling-restrained brace under cyclic loading calibrated to backbone curve. Note: E_c = initial concrete stiffness; f_c' = specified (design) compressive strength of concrete in psi units. 1 ksi = 6.89 MPa.

clear space between the transverse support hooks or hoops is less than $6d_b$, where d_b is the nominal diameter of the longitudinal reinforcing bar. This requirement was met for every beam and column based on the transverse reinforcement spacing from shear design and longitudinal reinforcing bar sizes from axial-flexural design. Thus, only the reinforcing bars in a beam or column with $P_u \leq 0.3A_g f_c'$ and not located at the corner of a hoop or seismic hook were considered to buckle (Fig. 4).

The two concrete material models included unconfined and confined concrete, represented using the Concrete01 and Concrete02 material types in OpenSees. The unconfined concrete material was used in the unconfined regions of each beam and column, which included the concrete cover, as well as the beam tributary topping slab. This model assumed a maximum concrete compressive strength f_c' of 6 ksi (41 MPa), the same as the concrete strength used in design. The confined concrete material represented the confined regions of the members bounded by the centerlines of the transverse hoop reinforcement. The maximum compressive strength of the confined concrete was calculated using the method by Mander et al.[32] based on the spacing and arrangement of the transverse reinforcement from ACI 318 section 22.5 requirements.

The post-peak compressive stress-strain relationships of the unconfined and confined concrete were determined following the regularization process developed by Coleman and Spacone,[33] Pugh et al.,[34] Vásquez et al.,[35] and Pozo et al.[36] to minimize the sensitivity of the softening concrete models (that is, with reducing stress beyond the maximum strength point) to the assumed critical integration lengths of the fiber beam and column elements. The residual post-peak concrete strength was assumed to be 20% of the maximum compressive strength. The regularization of the concrete post-peak compressive stress-strain relationships was performed using a plastic hinge length L_p taken as the average plastic hinge length calculated from the five equations listed in **Table 6**,[27,37–40] which was prescribed as the critical integration length of each element. Note that plastic hinge lengths for precast concrete members can differ from those of monolithic cast-in-place reinforced concrete structures due to different detailing and response of precast concrete members and connections.[41] However, the plastic hinge lengths calculated based on the equations in Table 6 were deemed appropriate for the purposes of this study because the archetype structures investigated were intended to emulate monolithic cast-in-place reinforced concrete structures. In addition, because the intent of the regularization of the concrete post-peak compressive stress-strain relationships is to minimize the sensitivity of the analysis results to the selected plastic hinge length (that is, critical integration length), models with concrete stress-strain relationships regularized based on different assumed plastic hinge lengths are expected to result in similar performance.[33–36]

Both Concrete01 and Concrete02 material models in OpenSees use a uniaxial Kent-Scott-Park nonlinear compressive stress-strain relationship. Linear unloading and reloading stiffness, equal to the initial stiffness E_c, was assumed for cyclic loading (Fig. 7). The maximum compressive strength, strain at maximum compressive strength, residual strength, and strain at residual strength are defined by the user, whereas the initial concrete stiffness E_c is implicitly calculated by OpenSees based on the user-defined maximum compressive strength and strain at maximum compressive strength. Because these material models do not allow the user to specify the concrete initial stiffness explicitly, the strain at maximum compressive strength was calculated to result in an initial concrete stiffness of $E_c = 57{,}000\sqrt{f_c'}$, with f_c' in psi units per ACI 318.

The only difference between Concrete02 and Concrete01 is that Concrete01 has zero tensile strength, whereas Concrete02 includes the tensile strength of the concrete. With Concrete02, the user defines the tensile strength and tension softening stiffness, in addition to the parameters used in Concrete01. The concrete in the beams was assumed to have tensile strength (Concrete02) equal to $7.5\sqrt{f_c'}$ (with f_c' in psi units per ACI 318), with the tensile stress conservatively assumed to drop immediately to zero after the initiation of cracking, thus ignoring any gradual tension softening. In comparison,

Table 6. Plastic hinge length equations

Equation	Units of measure	Reference
$L_p = 0.5d + \dfrac{0.032z}{\sqrt{d}}$	Meters	Corley (1966)
$L_p = 0.5d + 0.05z$	Any consistent length unit	Mattock (1967)
$L_p = 0.08z + 6d_b$	Any consistent length unit	Priestley and Park (1987)
$L_p = 0.08z + 0.022d_b f_{sy}$	Millimeters, megapascals	Paulay and Priestley (1992)
$L_p = 0.05z + \dfrac{0.1f_{sy}d_b}{\sqrt{f_c'}}$	Millimeters, megapascals	Berry et al. (2008)

Note: d = distance from extreme compression fiber to centroid of longitudinal reinforcement; d_b = nominal longitudinal reinforcing bar diameter; f_c' = specified (design) compressive strength of concrete; f_{sy} = specified (design) yield strength of reinforcing steel; L_p = plastic hinge length; z = distance from critical section of beam or column to point of contraflexure (assumed as ½ element length). 1 mm = 0.0394 in.; 1 m = 3.281 ft; 1 MPa = 0.145 ksi.

the column concrete was assumed to have no tensile strength (Concrete01), thus conservatively simulating the nonmonolithic (precast concrete) joints at the column ends (Fig. 6).

The buckling-restrained braces were modeled as nonlinear truss elements pinned between work point nodes without rigid end zones (Fig. 6) rather than with separate yielding and nonyielding regions of the brace. To properly account for the different regions of each brace with a single truss element, the element had an area equal to the yielding region of the brace (Table 4), and a stiffness modification factor was used to account for the increased stiffness from the relatively rigid end connection regions of each brace. The stiffness modification factors ranged from 1.35 to 1.90, depending on the geometry and yielding area of the brace. The equivalent backbone axial force–deformation curve for the work point–to–work point truss element was developed from the backbone curve for the yielding region and the equivalent areas for the nonyielding end regions of each brace. Cyclic characteristics (kinematic and isotropic hardening) were then selected such that the element behavior under cyclic loading would match the backbone curves (Fig. 7).

Frame modeling

Each archetype braced frame was simulated in OpenSees[17] using the aforementioned nonlinear elements and materials. The models had fixed column bases and fixed beam-to-column connections, but the column concrete was modeled with zero tensile strength (Concrete01), as noted in the previous section, to simulate the precast concrete joints. Tributary dead and live gravity loads were applied to the beams and columns of each archetype frame using the expected median gravity load combination of $1.05D + 0.25L$, as required by FEMA P695,[19] with live load reductions per ASCE 7-16[20] section 4.7. The gravity loads on each beam were applied as distributed loads based on tributary widths. The column gravity loads were modeled as point loads at the work point nodes at each floor and roof level. These loads were calculated from the column tributary areas and the loads in Table 1 but excluded the loads already applied to the beams in the model.

Because all of the gravity loads in a building (that is, not just the loads tributary to the braced frames) contribute to second-order P-Δ effects, a leaning column was connected to each frame model to capture the second-order effects of the gravity loads not already applied on the frame. This leaning column was pinned at the base and pinned at every three stories based on typical precast concrete column lengths in practice, with a pin-ended horizontal rigid link connection to the frame at each floor and roof work point node (**Fig. 8**). The additional building gravity loads were calculated as the total column axial loads in the gravity system of the building (that is, columns not part of the archetype braced frames). These loads were then summed and applied as point loads to the leaning column at each floor and roof level of the model. The leaning column was modeled as an elastic element with an assumed area equal to the sum of the cross-sectional areas and 70% of the sum of the moments of inertia of the gravity system columns based on ACI 318[23] Table 6.6.3.1.1(a). Because the gravity-resisting system of the building was not explicitly designed, each gravity load column was assumed to be 24 × 24 in. (610 × 610 mm) based on typical precast concrete practices.

For dynamic modeling, seismic masses were assigned to all of the work point nodes on the frame. As required by FEMA P695,[19] the total seismic mass for each floor and roof level of the entire building was calculated using the median gravity load combination of $1.05D + 0.25L$, with live load reductions per ASCE 7-16[20] section 4.7. The total building seismic mass was distributed equally between the braced frames in each direction, assuming rigid floor and roof diaphragms. Finally, the

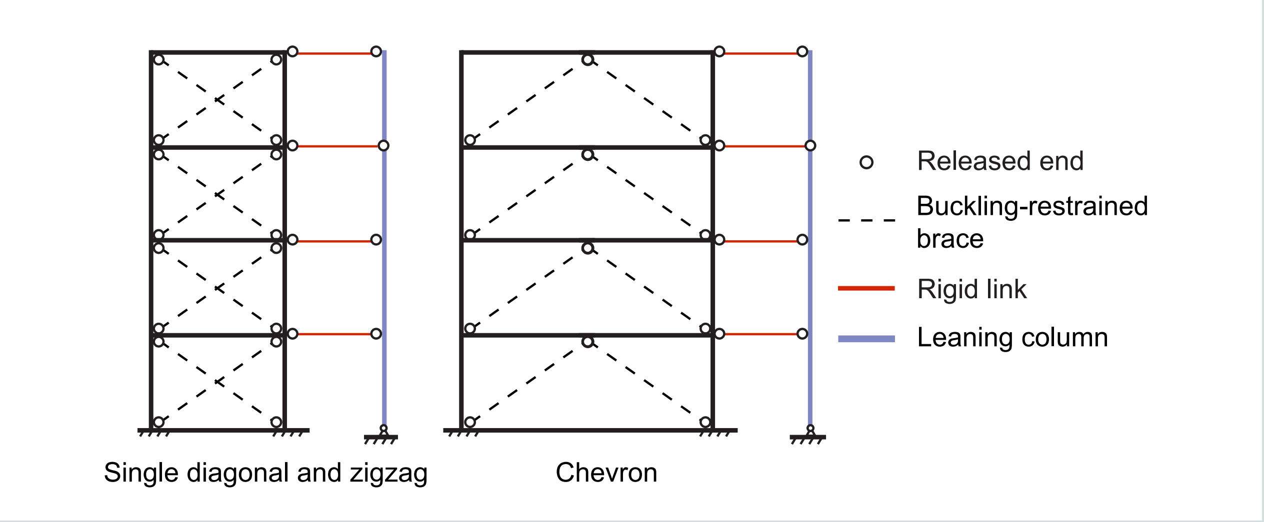

Figure 8. Braced-frame model elevation depicting leaning column and superimposed frames.

frame seismic mass at each floor and roof level was distributed equally between the two work point nodes at that level.

Depending on the brace configuration, the archetypes were modeled with one or two frames. The archetypes with chevron braces were modeled using a single braced frame to represent the building response. For the archetypes with zigzag and single-diagonal brace configurations, the lateral load behavior of a single frame was slightly different (that is, asymmetric) for the two in-plane loading directions. This difference stemmed from the asymmetric layout of the braces over the height of the frames. However, the overall building behavior was expected to remain essentially symmetric because an even number of frames were placed within the building plan with alternating brace orientations to avoid the asymmetry of a single frame. To simulate the expected symmetric behavior of the building as a whole, rather than the asymmetric behavior of a single frame, each zigzag and single-diagonal braced archetype was modeled using two superimposed frames (Fig. 8). These frames were identical except for the orientation of the braces. The analyses were conducted by subjecting the corresponding work point nodes (at the beam-to-column connections) of the two frames to the same lateral displacement history, assuming the presence of a rigid diaphragm at each floor and roof level of the building. Accordingly, the seismic masses and gravity loads for these models were also doubled for analysis.

Nonlinear model validation

The OpenSees[17] nonlinear modeling approach described in the previous section was validated using available experimental and numerical results from Guerrero et al.[15] and comparable numerical models developed using a second analysis platform, DRAIN-2DX.[18] The study by Guerrero et al. compared the dynamic properties and seismic responses of two four-story precast concrete frame test specimens, with and without buckling-restrained braces. The beam and column members and connections of the specimens used a combination of precast concrete and cast-in-place concrete, designed with practices used in Mexico. Braces were placed in a zigzag configuration over the four stories, with the ends of each brace laterally offset from the beam-to-column connections such that the braces were attached solely to the beams. The Ministry of Communications and Transportation building site east-west ground motion (SCT-EW) record from the 1985 Michoacán, Mexico, earthquake was used in the study. The structures, constructed at one-third scale, were subjected to low-intensity white noise and the SCT-EW record of the 1985 Michoacán earthquake at different scaling factors (up to two times the original record intensity) using a shake table. The study also included numerical analyses of the test specimens.

The OpenSees models of the test specimens from Guerrero et al. were developed following an approach similar to that used for the archetype frames. The material models for the concrete, reinforcing steel, and braces were based on the properties reported by Guerrero et al., including an additional Concrete02

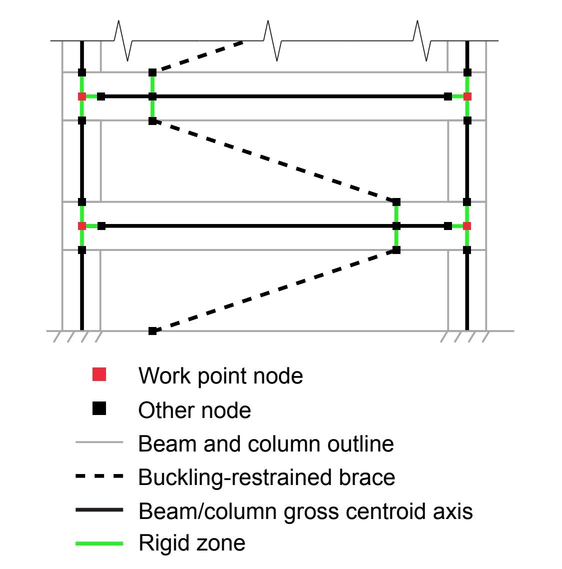

Figure 9. Modeling assumptions for precast concrete buckling-restrained braced frame tested by Guerrero et al. (2018).

material for the cast-in-place regions of each member. The properties of the confined concrete regions were calculated using the procedures of Mander et al.[32] based on the arrangement of the reinforcement in the test specimens. Both beams and columns were modeled with rigid end zones and concrete tensile strength (Concrete02) because the beam-to-column connections of the specimens in the study by Guerrero et al. did not have the precast concrete joints assumed for the archetypes herein. The brace elements were placed at 20 degrees from horizontal, with rigid end zones to represent the connections of each brace to the beam elements of the frame (**Fig. 9**).

These models were used to conduct nonlinear static pushover and dynamic analyses of the test specimens. Because the physical specimens were not subjected to pushover tests, the numerical base shear versus story drift behaviors from the models in this study were compared with the numerical pushover curves presented in Guerrero et al., which were also developed using OpenSees (**Fig. 10**). For dynamic analyses, the numerical results were compared with the experimentally measured roof displacement time history of the braced-frame specimen subjected to the SCT-EW record of the 1985 Michoacán earthquake.

In addition, **Fig. 11** compares the numerical peak dynamic response envelopes over the height of the braced-frame specimen with the experimental results from Guerrero et al. These comparisons show that the analyses conducted following the numerical modeling approach for the archetypes provided a good match to the measured peak story drift and floor displacement data for the test specimen. The discrepancies for the peak absolute velocities and accelerations were generally larger, which may be expected for nonlinear dynamic modeling because they are higher-order responses. However, because the peak drift and displacement responses

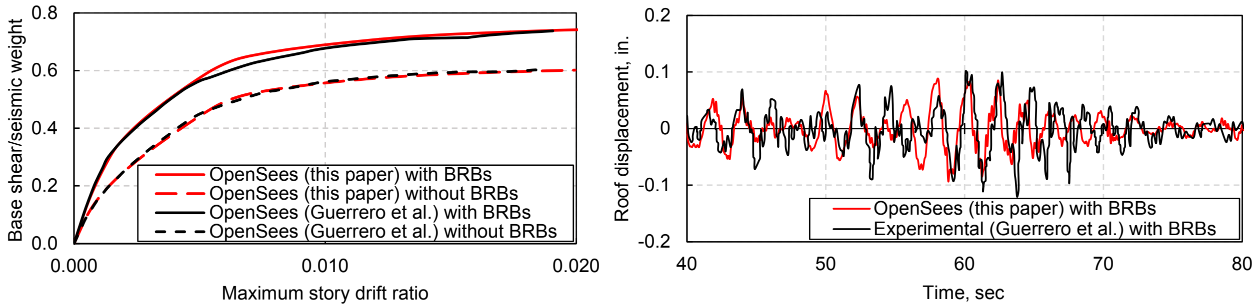

Figure 10. Comparisons of pushover curves (left) and dynamic roof displacement response (right, subjected to the Ministry of Communications and Transportation building site east-west ground motion record at 100%) with results from Guerrero et al. Note: BRB = buckling-restrained brace. 1 in. = 25.4 mm.

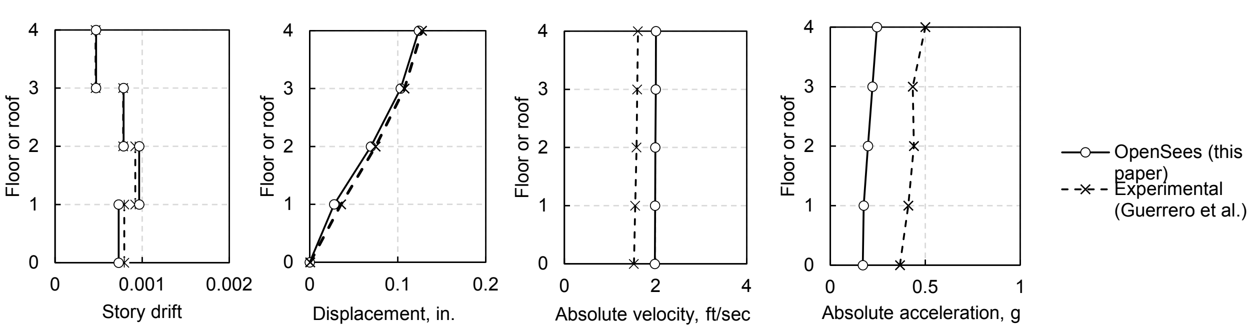

Figure 11. Comparisons of absolute peak dynamic response envelopes of braced-frame test specimen (subjected to the Ministry of Communications and Transportation building site east-west ground motion record at 100%) with results from Guerrero et al. Note: g = gravitational acceleration. 1 in. = 25.4 mm; 1 ft = 0.305 m.

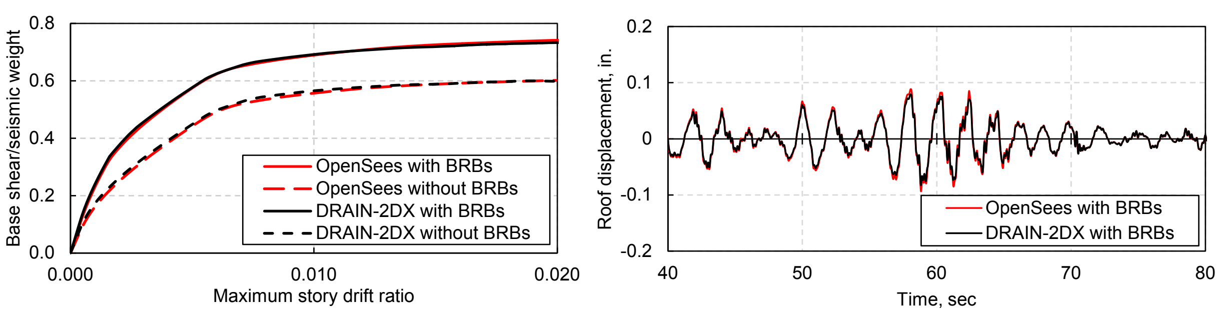

Figure 12. Comparisons of OpenSees and DRAIN-2DX model pushover curves (left) and dynamic roof displacement response (right, (subjected to the Ministry of Communications and Transportation building site east-west ground motion record at 100%) of the test specimens from Guerrero et al. Note: 1 in. = 25.4 mm.

are the most important dynamic results for the FEMA P695[19] evaluation, the validations of the modeling approach herein demonstrated the suitability of the models for the purposes of the study described in this paper.

For further validation, the OpenSees analyses of the test specimens were compared with results obtained using nonlinear models in a second structural analysis program, DRAIN-2DX. All elements in DRAIN-2DX were also modeled with fiber sections, and the concrete and steel materials were modeled to match the OpenSees models as closely as possible. **Figure 12** shows that the results from the two modeling programs were nearly identical for the nonlinear pushover analyses as well as the dynamic response history analyses of the specimens. These comparisons provided further confidence for the use of the OpenSees models in the FEMA P695 study described in this paper.

Linear-elastic drift model validation

In addition to the FEMA P695[19] evaluation of the archetypes, the OpenSees[17] nonlinear braced-frame model was also used to validate the equivalent lateral force level deformations of the effective linear-elastic drift model used in design. To perform this validation, both the nonlinear model and the effective linear-elastic drift model for each archetype were subjected to the same equivalent lateral forces used in design, and the resulting roof drifts were compared. Because the gravity loads from ASCE 7-16[20] load combination 7 governed the drift design from the effective linear-elastic drift models, the corresponding nonlinear models were also subjected to the same gravity loads from load combination 7.

Figure 13 shows that the stiffness reduction factors in Table 5 resulted in good or reasonable estimations of the nonlinear roof drifts at the equivalent lateral force level for three selected archetypes. The effective stiffness models of the archetypes that were drift controlled during design (all of these cases were for nine-story archetypes) tended to underestimate the nonlinear model drifts at the equivalent lateral force level (see pushover curves for archetype 2SD9 in Fig. 13). Because the column dimensions of the drift-controlled archetypes were increased to meet the ASCE 7-16 drift requirements (see the "Design of Archetypes" section in this paper), the longitudinal reinforcement ratios in these structures were relatively low, around 2%, whereas most of the other archetypes had reinforcement ratios around 4% to 5%. Therefore, the stiffness reduction factors in Table 5 may be better calibrated to column reinforcement ratios of around 4% to 5%. This discrepancy, however, was deemed acceptable given that the errors were not large and that only five of the archetypes were drift controlled during design. It may be possible to eliminate drift-controlled designs by using prestressed beam and column members to reduce cracking; however, this design option was not investigated.

Archetype performance evaluation and results

Each archetype braced frame was subjected to static pushover and dynamic response time-history analyses using the validated nonlinear OpenSees[17] numerical model described previously in this paper. These analyses and the evaluations of the results followed the FEMA P695[19] methodology. The pushover analysis results were used to determine the system overstrength factor Ω_0 and period-based ductility μ_T, whereas the dynamic analysis results were evaluated with respect to the response modification coefficient R and deflection amplification factor C_d used in design. The results for the 32 archetypes are summarized in **Table 7**. The procedures used for analysis, including the dynamic response parameters and collapse criteria used in the seismic evaluation, are described next, followed by discussions of the results in Table 7.

Dynamic response parameters and collapse criteria

The results of the FEMA P695[19] procedure rely heavily on the response parameters determined from the numerical analyses

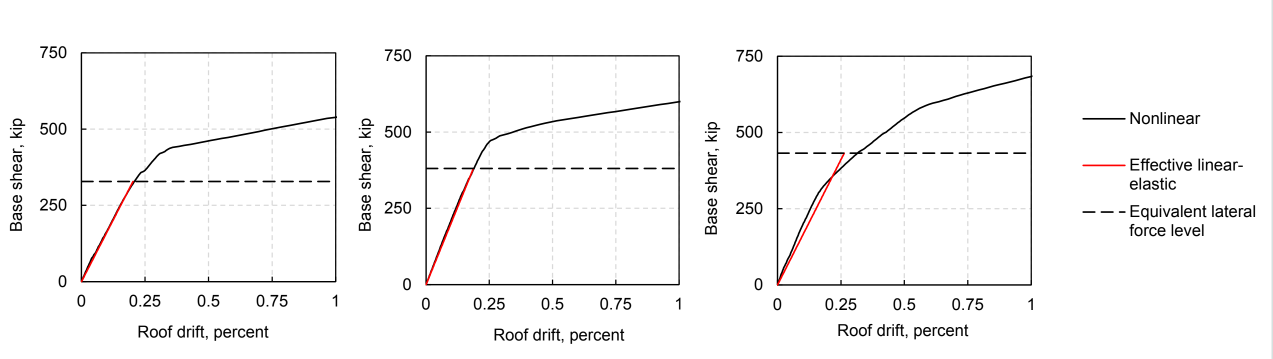

Figure 13. Comparison of effective linear-elastic drift model and nonlinear model monotonic pushover curves for archetypes 1SD3 (left), 2CC3 (center), and 2SD9 (right). Note: CC = chevron brace configuration; SD = single-diagonal brace configuration. 1 kip = 4.45 kN.

Table 7. Summary of pushover and dynamic analysis results

Performance Group	Archetype design identification number	Design configuration		Overstrength and collapse parameters			Acceptance check	
		Number of stories	Seismic design category	Ω_0	μ_T	ACMR	ACMR limit†	Pass/fail
1	1SD1	1	D_{max}	2.94	7.35	1.89	1.56	Pass
	1SD2	2		2.29	7.55	2.55	1.56	Pass
	1SD3	3		2.19	8.43	2.65	1.56	Pass
	Performance group mean			2.47	7.78	2.36	1.96	Pass
2	2SD1	1	D_{max}	2.97	7.01	1.61	1.56	Pass
	2SD2	2		2.30	8.28	1.78	1.56	Pass
	2SD3	3		2.09	8.79	1.73	1.56	Pass
	4SD1	1		2.78	7.61	2.42	1.56	Pass
	4SD2	2		2.24	9.57	2.32	1.56	Pass
	Performance group mean			2.48	8.25	1.97	1.96	Pass
3	1SD6	6	D_{max}	2.14	7.34	3.02	1.56	Pass
	1SD9	9		2.13	7.11	2.15	1.56	Pass
	2SD6	6		2.04	7.64	2.13	1.56	Pass
	2SD9	9		2.31	7.50	1.86	1.56	Pass
	Performance group mean			2.15	7.40	2.29	1.96	Pass
4	3SD1	1	D_{min}	2.79	7.65	2.31	1.56	Pass
	3SD2	2		2.34	8.23	2.67	1.56	Pass
	3SD3	3		2.28	7.77	2.89	1.96	Pass
	Performance group mean			2.47	7.88	2.62	1.56	Pass
5*	2CC1	1	D_{max}	2.04	8.49	1.77	1.56	Pass
	2CC2	2		1.97	7.84	2.01	1.56	Pass
	2CC3	3		1.89	8.22	2.07	1.56	Pass
	5CC1	1		2.05	8.97	2.55	1.56	Pass
	5CC2	2		2.00	9.11	2.32	1.56	Pass
	Performance group mean			1.99	8.53	2.14	1.96	Pass
6	2CC4	4	D_{max}	1.87	8.87	2.24	1.56	Pass
	2CC6	6		1.78	8.14	2.59	1.56	Pass
	2CC9	9		1.76	7.34	2.68	1.56	Pass
	Performance group mean			1.80	8.12	2.50	1.96	Pass
7	3CC1	1	D_{min}	2.27	9.03	1.86	1.56	Pass
	3CC2	2		1.94	9.74	2.82	1.56	Pass
	3CC3	3		1.76	10.72	2.95	1.56	Pass
	Performance group mean			1.99	9.83	2.54	1.96	Pass
8*	2ZZ2	2	D_{max}	2.42	7.99	2.20	1.56	Pass
	2ZZ3	3		2.11	8.68	2.13	1.56	Pass
	4ZZ2	2		2.14	9.61	2.66	1.56	Pass
	Performance group mean			2.22	8.76	2.33	1.96	Pass
9	2ZZ4	4	D_{max}	2.02	8.46	2.07	1.56	Pass
	2ZZ6	6		1.96	7.88	2.14	1.56	Pass
	2ZZ9	9		2.14	7.93	2.03	1.56	Pass
	Performance group mean			2.04	8.09	2.08	1.96	Pass

Note: ACMR = adjusted collapse margin ratio; CC = chevron brace configuration; SD = single-diagonal brace configuration; ZZ = zigzag brace configuration; μ_T = period-based ductility; Ω_0 = system overstrength factor.

*These performance groups were evaluated using a less-conservative definition of maximum brace ductility (see "Dynamic Response Parameters and Collapse Criteria" section of paper).

† The ACMR limit listed for the individual archetypes is for 20% collapse probability, and the ACMR limit listed for the performance group mean is for 10% collapse probability. Per FEMA P695, the value of the response modification coefficient *R* used in design is deemed acceptable when both of the following conditions are satisfied: the average ACMR for the archetypes in each performance group is greater than or equal to the 10% ACMR limit and the ACMR value for each archetype is greater than or equal to the 20% ACMR limit.

and the collapse criteria used in the seismic evaluation. The collapse criteria include failure types that are directly simulated during the numerical analysis, as well as nonsimulated failure types determined during the postprocessing of the analysis results. The failure types considered for the braced-frame archetypes in this study were brace failure, gravity load system failure, shear failure of the precast concrete beams and columns, and axial-flexure failure of the beams and columns.

Brace failure Brace failure was the most common collapse criterion governing the FEMA P695[19] evaluation results, which may be expected because braces are the primary yielding lateral-force-resisting members of this system. In this criterion, the structure was deemed to have failed when a brace exceeded the limit for its maximum ductility μ_{max} or its maximum cumulative inelastic ductility μ_c during the dynamic analysis. These brace ductility parameters were defined as

$$\mu_{max} = \Delta_{max}/\Delta_{by}$$

and

$$\mu_c = \Sigma\Delta_{inelastic}/\Delta_{by}$$

where

Δ_{max} = maximum brace deformation

$\Delta_{inelastic}$ = inelastic brace deformation

Δ_{by} = brace deformation at yield

The maximum brace ductility limits used in this study ranged from 17 to 20 in both compression and tension based on the performance of braces that have been tested in accordance with the cyclic qualification requirements in ANSI/AISC 341-16[25] section K3. The cumulative ductility limit was conservatively set as 200, which is the minimum cumulative ductility required for cyclic qualification testing, though the performance of braces tested in accordance with ANSI/AISC 341-16 would support much higher values.

The maximum cumulative inelastic ductility limit of the braces did not control the seismic performance of the archetypes. In comparison, the maximum ductility limit governed the primary failure mode. Because the maximum ductility limit values used in the evaluation were based on the performance of braces tested in accordance with minimum ANSI/AISC 341-16 requirements, these limits also represented conservative (lower) values for actual expected brace ductility capacities. In other words, the actual ductility capacity of a brace under a ground motion record was expected to exceed the performance of the brace from ANSI/AISC 341-16 cyclic qualification testing because the testing procedures require extremely rigorous strain cycles that are not likely to occur under typical earthquake events. Therefore, a revised (less conservative) collapse criterion for brace ductility was used for a few of the archetypes that did not initially pass the FEMA P695 requirements when using maximum ductility limits based on measured brace performance from minimum ANSI/AISC 341-16 requirements. In this revised definition, brace failure was based on the total ductility range of the brace rather than the absolute ductility in either direction (that is, compression or tension) of loading. This ductility range was calculated as the difference between the overall maximum and minimum brace ductility over its entire loading history. For example, consider a brace with a maximum ductility limit of ±17 established from ANSI/AISC 341-16 cyclic qualification testing. If this brace experienced a tension ductility demand of +25 and a compression ductility demand of -5 during an earthquake, the corresponding total maximum ductility demand range would be calculated as 25 – (-5) = 30. In this example, the maximum brace ductility demand of 25 exceeds the maximum ductility limit of 17; however, the brace is deemed not to have reached failure because the total range of ductility demand (30) remains under the maximum ductility range limit of 34, calculated as twice the maximum ductility limit of 17 (that is, maximum ductility range of 17 – [-17] = 34). The archetypes in performance groups 5 and 8 were all evaluated based on this less-conservative collapse criterion (Table 7).

To ensure that the revised definition of maximum brace ductility failure criterion was still conservative, the most critical braces from the archetypes were further checked for fatigue failure. This was done by evaluating the strain history of a brace over the entire dynamic analysis (from the FEMA P695 study) with a fatigue life model (between strain and number of cycles to failure) developed through testing by the brace manufacturer and the University of California San Diego, as documented in Saxey et al.[42] This analysis provided a damage index for each brace, calculated based on standard rainflow counting of the strain reversals of the brace over the duration of the ground motion; a damage index at or above 100% would indicate brace failure. The results showed a maximum damage index of only 16% for even the most critical cases from the archetypes in this study. Thus, the braces were deemed very unlikely to fail under the FEMA P695 ground-motion record set before the collapse criteria outlined in this paper, and the revised definition of maximum brace ductility failure was deemed adequate.

Note that because maximum brace deformation limits are based on the strain capacities of the yielding region, braces with shorter yielding lengths tend to be less deformable and could reach failure earlier than longer braces. Thus, frame dimensions that result in shorter brace yielding lengths than those investigated in this paper (Table 4) may be more susceptible to collapse.

Gravity load system failure Gravity load system failure was deemed to occur at a prescribed story drift of 5% for any story. This requirement is consistent with other FEMA P695 studies (for example, Bruneau et al.[43] and Tauberg et al.[44]), where 5% drift was expected to correspond to extensive damage to a structure.

Shear failure of beams and columns Shear failure was checked by comparing the maximum shear force demands in the beam and column members against the corresponding shear strengths calculated using ACI 318[23] section 22.5.5. The analysis results showed that this failure criterion did not govern the collapse of any of the archetypes.

Axial-flexural failure of beams and columns Excessive axial-flexural damage to the beams and columns of each frame was also considered as a collapse criterion. This excessive damage was defined as the crushing of concrete in any beam or column over a depth equal to 25% of the beam or column depth, or buckling or fracture of the extreme layer of longitudinal reinforcement in any beam or column. These criteria did not govern the collapse of the archetypes.

System overstrength factor Ω_0 and period-based ductility μ_T

The nonlinear static pushover analyses provided data on the system overstrength factor Ω_0 and period-based ductility μ_T for each archetype frame. Per FEMA P695,[19] the vertical distribution of the lateral forces at the floor and roof levels was determined based on the seismic mass and the ordinate of the fundamental mode for the frame model at each level. As an example, **Fig. 14** shows the monotonic pushover analysis curve for archetype 1SD2. Although not required by FEMA P695, the behavior of the structure under reversed-cyclic lateral loads is also shown. For each archetype, the overstrength factor was calculated as the ratio of the maximum base shear strength V_{max} (from a monotonic analysis) to the design base shear force V_{ELF}. Based on the results in Table 7, the overstrength factor for the precast concrete buckling-restrained brace system Ω_0 was calculated as 2.5, taken as the largest average overstrength factor out of all the performance groups, rounded up to the next half-unit interval.

Period-based ductility μ_T was calculated as the ratio of the ultimate roof drift δ_u to the effective yield roof drift $\delta_{y,eff}$, where roof drift was calculated as the lateral displacement at the roof level divided by the height of the archetype. The ultimate roof drift was determined from the roof displacement at the predicted failure of the frame, usually corresponding to the maximum ductility limit of the braces (see the "Dynamic Response Parameters and Collapse Criteria" section in this paper). Effective yield roof drift was calculated as the linear elastic roof drift of the structure at the maximum base shear strength V_{max}. Based on the results of Table 7, period-based ductility μ_T exceeded 6 for all of the archetypes, and the system had an average ductility of 8.2.

System response modification coefficient *R*

The response modification coefficient *R* of 8 used in the design of the archetypes was evaluated based on the results of the nonlinear dynamic response history analyses. Per FEMA P695,[19] these analyses were conducted according to a modified incremental dynamic analysis procedure (Vamvatsikos and Cornell[45]), where each model was subjected to a set of ground motion records at increasing (scaled) intensities until the structure was deemed to reach collapse. FEMA P695 prescribes a set of 22 far-field ground motion pairs (44 records total) curated from the Pacific Earthquake Engineering Research Center Next-Generation Attenuation database[46] to assess collapse. These ground motion records were normalized by their respective peak ground velocities, and then the entire record set was collectively multiplied with increasing scaling factors under the requirements of the FEMA P695 methodology. Specifically, FEMA P695 characterizes ground motion intensity based on the spectral acceleration at the fundamental period of the archetype, with the important distinction that this intensity is defined collectively by the median spectral acceleration of the entire record set (**Fig. 15**), rather than by the different spectral accelerations of the individual records in the set.

The fundamental period *T* used to determine the median intensity is based on the maximum allowed ASCE 7-16[20] fundamental period C_uT_a for each archetype, not the period comput-

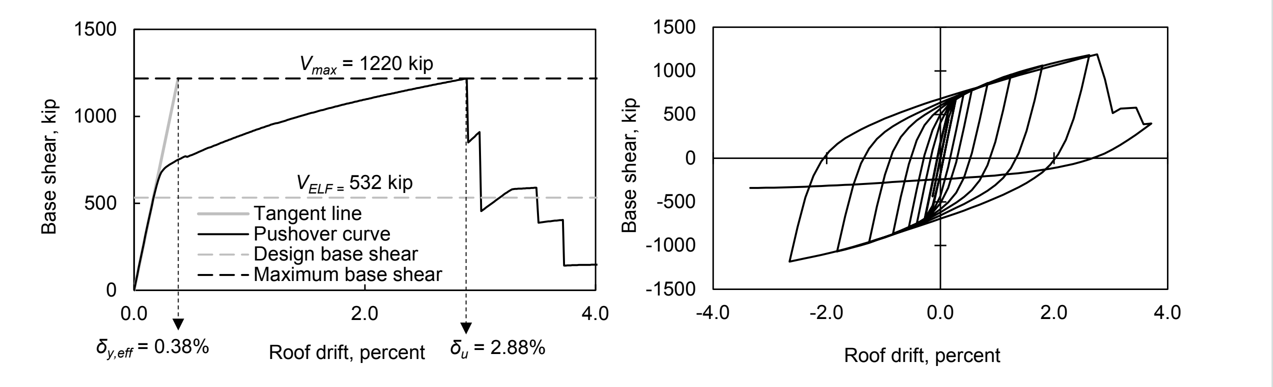

Figure 14. Monotonic pushover curve (left) showing parameters for calculation of overstrength and ductility and cyclic pushover curve (right) for archetype 1SD2. Note: SD = single-diagonal brace configuration; V_{ELF} = design base shear force; V_{max} = maximum base shear strength; δ_u = ultimate roof drift; $\delta_{y,eff}$ = effective yield roof drift. 1 kip = 4.45 kN.

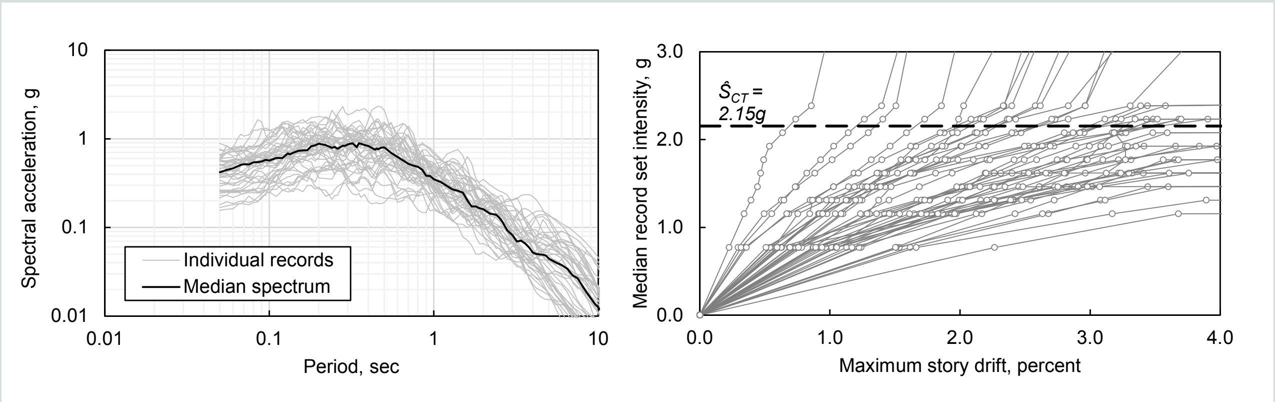

Figure 15. Acceleration response spectra of the normalized Federal Emergency Management Agency's *Quantification of Building Seismic Performance Factors*, FEMA P695, record set (left) and sample incremental dynamic analysis results for archetype 1SD1 (right). Note: g = gravitational acceleration; SD = single-diagonal brace configuration. $\hat{S}_{CT}$ = median collapse intensity.

ed from a numerical model of the structure using eigenvalue analysis. According to FEMA P695, normalizing and then collectively scaling the records leads to a range of spectral accelerations across the record set at the fundamental period of the structure in a manner that maintains overall record-to-record variability while eliminating inherent differences from factors such as event magnitude and distance to source.

Per FEMA P695, the lowest intensity (that is, lowest median spectral acceleration of the collective record set) that is deemed to cause collapse of an archetype under half (22) of the records was taken as the median collapse intensity $\hat{S}_{CT}$. This approach can be represented in an incremental dynamic analysis response plot of median spectral acceleration and maximum story drift, as shown for archetype 1SD1 in Fig. 15. In this figure, each gray line represents the maximum story drift response of the archetype model under one ground motion record at increasing intensities, where each point represents the dynamic analysis result from one record at one intensity. Failure of the archetype (based on the aforementioned collapse criteria) during a ground motion event is usually manifested in the graph as the flattening of the response curve under increasing intensities. The $\hat{S}_{CT}$ value corresponds to the median intensity at which the structure is deemed to have collapsed under half of the records. After $\hat{S}_{CT}$ is determined, the corresponding collapse margin ratio (CMR) is calculated as

$$\text{CMR} = \hat{S}_{CT}/S_{MT}$$

where

S_{MT} = maximum considered earthquake intensity from the response spectrum at the fundamental period of the structure T per ASCE 7-16[20] section 11.4.4

The adjusted collapse margin ratio (ACMR) is then calculated by multiplying the CMR with a spectral shape factor (SSF) as defined by FEMA P695 Tables 7-1a or 7-1b. The SSF, determined based on period-based ductility μ_T and fundamental period T for the archetype, is intended to account for ground motions that differ from the ASCE 7-16 design spectrum.

To evaluate the response modification coefficient R of 8 used in design, the collapse performance of each archetype was assessed based on the ACMR value from the incremental dynamic analysis procedure. For this evaluation, FEMA P695 Table 7-3 provides minimum ACMR limits corresponding to 10% and 20% collapse probabilities based on the total system collapse uncertainty β_{TOT} calculated using the following equation.

$$\beta_{TOT}^{\,2} = \beta_{RTR}^{\,2} + \beta_{DR}^{\,2} + \beta_{TD}^{\,2} + \beta_{MDL}^{\,2}$$

where

β_{RTR} = record-to-record variability = $0.20 \le 0.1 + 0.1\mu_T \le 0.40$

β_{DR} = uncertainty in design requirements

β_{TD} = test data uncertainty

β_{MDL} = modeling uncertainty

Values for the total system collapse uncertainty β_{TOT} range from 0 to 1. The expected uncertainty values in design requirements, test data, and modeling are all based on a qualitative assessment of each uncertainty and FEMA P695 Tables 3-1, 3-2, and 5-3. In this study, all three uncertainties were rated as "good," corresponding to $\beta_{DR} = \beta_{TD} = \beta_{MDL} = 0.20$. Based on these results, the total system collapse uncertainty β_{TOT} is 0.53, and the corresponding minimum ACMR limits were calculated as 1.56 and 1.96 for 20% and 10% collapse probabilities, respectively.

Per FEMA P695, the value for the response modification coefficient R used in design is deemed acceptable when both of the following conditions are satisfied:

- The average ACMR for the archetypes in each performance group is greater than or equal to the 10% ACMR limit.

- The ACMR value for each archetype is greater than or equal to the 20% ACMR limit.

Table 7 shows that the calculated individual and average ACMR values for all of the archetypes were above the ACMR limits based on 10% and 20% collapse probabilities. The response modification coefficient R value of 8 used in design was therefore deemed acceptable for the precast concrete buckling-restrained braced-frame system.

System deflection amplification factor C_d

According to FEMA P695,[19] the system deflection amplification factor C_d is calculated as

$$C_d = R/B_I$$

where

B_I = numerical coefficient for effective damping β_I from Table 18.7-1 of ASCE 7-16[20]

β_I = effective damping due to inherent dissipation of energy by the structure, at or just below the effective yield displacement of the seismic-force-resisting system (ASCE 7-16 section 18.7.3.2)

FEMA P695 assumes that the structure will have inherent damping at 5% of critical. Therefore, the numerical coefficient for effective damping B_I is 1.0 for the system, and deflection amplification factor $C_d = R = 8$.

An explicit calculation of the deflection amplification factor C_d for each archetype was also performed to justify the value of 8. This alternate calculation of deflection amplification factor C_d was based on a method performed by other FEMA P695 studies, including Bruneau et al.[43] and Tauberg et al.[44] In this method, the deflection amplification factor C_d is calculated as

$$C_d = \delta_{DBE}/\delta_{ELF}$$

where

δ_{DBE} = maximum dynamic roof drift demand at design earthquake intensity

δ_{ELF} = roof drift of effective linear-elastic drift model under equivalent lateral forces

The value of the maximum dynamic roof drift demand at the design earthquake intensity δ_{DBE} for each archetype was determined using the following steps:

1. Scale the median spectral acceleration of the FEMA P695 collective ground-motion record set to the design earthquake spectrum level at the fundamental period of the archetype C_uT_a, where the design earthquake intensity is determined from FEMA P695 based on the seismic design category (SDC).

2. Conduct nonlinear dynamic history analyses of the structure under each scaled record.

3. Find the maximum roof drift demand from each record.

4. Take the median value across all of the maximum roof drift demands as the maximum dynamic roof drift demand at the design earthquake intensity δ_{DBE}.

The roof drift of the effective linear-elastic drift model under equivalent lateral forces δ_{ELF} was determined for each archetype with the gravity loads changed to the FEMA P695 median load combination of $1.05D + 0.25L$. The purpose of using the effective linear-elastic drift model rather than the nonlinear model was for the resulting roof drift δ_{ELF} to be consistent with the value used in the design of each archetype. The results of these calculations are outlined in **Table 8**, showing that the deflection amplification factor C_d across all archetypes ranged from 3.9 to 9.8. The mean C_d values for the different performance groups ranged from 4.9 to 7.5, and thus, the results of this alternate method supported the recommended system level deflection amplification factor C_d value of 8.

Note that although a deflection amplification factor C_d of 8 is recommended to encompass a wide range of applications for the proposed precast concrete braced-frame system, archetypes with a higher number of stories typically resulted in lower values of the deflection amplification factor C_d. For example, all archetypes with six stories or more had deflection amplification factor C_d values close to 5 (Table 8). Thus, future work may consider separating the precast concrete buckling-restrained braced-frame system based on the number of stories or height to allow for the use of a lower deflection amplification factor C_d value for taller buildings. This would be beneficial for design because taller buildings are more likely to be controlled by drift, and thus, more efficient designs can be achieved using a lower deflection amplification factor C_d value for these structures.

Conclusion

This study numerically evaluated the seismic design of precast concrete buckling-restrained braced frames as a novel primary lateral-force-resisting structure using the FEMA P695[19] methodology. A set of 32 braced-frame archetypes were designed to represent the range of key parameters expected to govern the seismic performance of the system, including the brace configuration (chevron, single diagonal, and zigzag), building height, and building layout. Nonlinear static pushover analyses of the structures were conducted to determine the system overstrength factor Ω_0. In addition, incremental dynamic analyses were conducted under a set of

Table 8. Calculated deflection amplification factors

Performance group	Archetype design identification number	Design configuration		C_d
		Number of stories	Seismic design category	
1	1SD1	1	D_{max}	8.7
	1SD2	2		7.3
	1SD3	3		6.4
	Performance group mean			7.5
2	2SD1	1	D_{max}	8.6
	2SD2	2		6.7
	2SD3	3		6.0
	4SD1	1		6.5
	4SD2	2		6.8
	Performance group mean			6.9
3	1SD6	6	D_{max}	4.8
	1SD9	9		5.1
	2SD6	6		4.8
	2SD9	9		5.0
	Performance group mean			4.9
4	3SD1	1	D_{min}	9.2
	3SD2	2		5.9
	3SD3	3		3.9
	Performance group mean			6.3
5	2CC1	1	D_{max}	8.6
	2CC2	2		6.8
	2CC3	3		6.5
	5CC1	1		7.0
	5CC2	2		7.6
	Performance group mean			7.3
6	2CC4	4	D_{max}	6.6
	2CC6	6		5.4
	2CC9	9		4.3
	Performance group mean			5.4
7	3CC1	1	D_{min}	9.8
	3CC2	2		6.1
	3CC3	3		4.4
	Performance group mean			6.8
8	2ZZ2	2	D_{max}	7.0
	2ZZ3	3		6.2
	4ZZ2	2		7.1
	Performance group mean			6.8
9	2ZZ4	4	D_{max}	6.1
	2ZZ6	6		5.0
	2ZZ9	9		5.1
	Performance group mean			5.4

Note: C_d = deflection amplification factor; CC = chevron brace configuration; SD = single-diagonal brace configuration; ZZ = zigzag brace configuration.

44 ground motion records to evaluate the response modification coefficient R and deflection amplification factor C_d used in design. The main conclusions from the study are as follows:

- Buckling-restrained braces exert large axial tension forces on the beams and columns, which result in large reinforcement requirements for these members. The use of higher-grade reinforcing bars can minimize the sizes of the beam and column members while meeting design requirements for steel reinforcement ratios.

- The large axial forces (both tension and compression) that develop in the beams of buckling-restrained precast concrete frames require these members to be designed and detailed like columns of special reinforced concrete frames.

- Current practice for the design of buckling-restrained braces in steel frames is typically based on brace deformations calculated using a simplified shear building model where the beam and column members of the frame are assumed to be axially rigid. This assumption can lead to unrealistically large brace elongations in precast concrete braced frames because it ignores the frame deformations due to cracked beams and columns. As such, buckling-restrained braces in precast concrete frames should be designed using the brace deformations calculated directly from an effective (cracked) linear-elastic drift analysis model. This paper provides recommended effective stiffness reduction factors for beams and columns that can be used for design.

- The nonlinear numerical modeling approach described in this paper provided good comparisons with available experimental shake-table test results of a precast concrete buckling-restrained braced frame, especially in terms of the peak displacement response parameters, which are most important for the FEMA P695 evaluation. These comparisons provided the validation of the models used in this paper.

- The numerical analyses showed that typical failure of the archetype frames was reached due to failure of the buckling-restrained braces by exceeding maximum brace ductility limits. In comparison, the maximum cumulative inelastic ductility limit of the braces or the failure of the beams and columns did not govern the seismic performance of the archetypes.

- Based on the nonlinear pushover and dynamic analyses of the archetype frames in this study, the proposed system overstrength factor Ω_0 is 2.5, response modification coefficient R is 8, and deflection amplification factor C_d is 8 for precast concrete buckling-restrained frames. These proposed seismic performance factors were shown to satisfy the applicable FEMA P695 collapse probability limits for a variety of building plans, building heights, and brace configurations.

Note that these conclusions may be limited to the archetypes designed, the assumptions made in their numerical modeling and collapse criteria, and the ground motion records used in the dynamic analyses. The precast concrete buckling-restrained braced-frame system currently lacks United States–based experimental evaluation, so future work is needed to provide system-level test data for this novel structure. In addition, this study did not include the design of the brace connections to the beam and column members. Future experimental testing is needed to ensure that these connections can be properly designed and detailed to reach the system performance levels shown in this study. Future work should also explore the use of buckling-restrained braces within prestressed and jointed (that is, nonemulative) precast concrete structures. Finally, based on the trends shown in the rigorous calculation of the deflection amplification factor C_d, future work may consider separating the system with respect to height, to allow for the use of a more favorable (lower) deflection amplification factor C_d value for taller buildings (for example, using a deflection amplification factor C_d of 5 for structures with 6 or more stories).

Acknowledgments

This research was conducted with the sponsorship of PCI under a Daniel P. Jenny Research Fellowship. The authors acknowledge the support of the PCI Research and Development Council, the PCI Central Region, and the members of the Industry Advisory Committee, including Keith Bauer of Buehler Engineering Inc., Roger Becker of PCI (retired), Kal Benuska of John A. Martin & Associates Inc., Jared Brewe of PCI, S. K. Ghosh of S. K. Ghosh Associates, Harry Gleich of Metromont Corp., Kevin Kirkley of Tindall Corp., Laura Redmond and Brandon Ross of Clemson University, Kim Seeber of Seaboard Services of Virginia Inc., and Jeff Viano of Simpson Gumpertz & Heger Inc. Any opinions, findings, conclusions, and recommendations expressed in the paper are those of the authors and do not necessarily reflect the views of the individuals and organizations acknowledged herein.

References

1. Watanabe, A., Y. Hitomi, E. Saeki, A. Wada, and M. Fujimoto. 1988. "Properties of Brace Encased in Buckling-Restraining Concrete and Steel Tube." In *Proceedings of the 9th World Conference on Earthquake Engineering*, vol. 4, 719–724. https://www.iitk.ac.in/nicee/wcee/article/9_vol4_719.pdf.

2. Tremblay, R., G. Degrange, and J. Blouin. 1999. "Seismic Rehabilitation of a Four-Storey Building with a Stiffened Bracing System." In *Proceedings of the 8th Canadian Conference on Earthquake Engineering*, 549–554. Vancouver, BC: Canadian Association for Earthquake Engineering.

3. Merritt, S., C. M. Uang, and G. Benzoni. 2003. *Subassemblage Testing of CoreBrace Buckling-Restrained Braces*. Structural Systems Research Project report TR-2003/04. La Jolla, CA: University of California San Diego.

4. Black, C. J., N. Makris, and I. D. Aiken. 2004. "Component Testing, Seismic Evaluation and Characterization of Buckling-Restrained Braces." *Journal of Structural Engineering* 130 (6): 880–894. https://doi.org/10.1061/(ASCE)0733-9445(2004)130:6(880).

5. Andrews, B. M., L. A. Fahnestock, and J. Song. 2009. "Ductility Capacity Models for Buckling-Restrained Braces." *Journal of Constructional Steel Research* 65: 1712–1720. https://doi.org/10.1016/j.jcsr.2009.02.007.

6. Clark, P., I. D. Aiken, E. Ko, K. Kasai, and I. Kimura. 1999. "Design Procedures for Buildings Incorporating Hysteretic Damping Devices." In *Proceedings of the 68th Annual Convention of the Structural Engineers Association of California*, 355–371. Sacramento, CA: SEAOC (Structural Engineers Association of California).

7. Clark, P., K. Kasai, I.D. Aiken, and I. Kimura. 2000. "Evaluation of Design Methodologies for Structures Incorporating Steel Unbonded Braces for Energy Dissipation." In *Proceedings of the 12th World Conference on Earthquake Engineering*. Upper Hutt, New Zealand: New Zealand Society for Earthquake Engineering. https://www.iitk.ac.in/nicee/wcee/article/2240.pdf.

8. Sabelli, R., S. Mahin, and C. Chang. 2003. "Seismic Demands on Steel Braced-Frame Buildings with Buckling-Restrained Braces." *Engineering Structures* 25: 655–666.

9. AISC (American Institute of Steel Construction) and SEAOC. 2001. *Recommended Provisions for Buckling-Restrained Braced Frames*. Chicago, IL: AISC.

10. ASCE (American Society of Civil Engineers) and SEI (Structural Engineering Institute). 2005. *Minimum Design Loads for Buildings and Other Structures*. ASCE/SEI 7-05. Reston, VA: ASCE.

11. Ishii, T., T. Mukai, H. Kitamura, T. Shimizu, K. Fujisawa, and Y. Ishida. 2004. "Seismic Retrofit for Existing R/C Building Using Energy Dissipative Braces." In *Proceedings of the 13th World Conference on Earthquake Engineering*, paper 1209. https://www.iitk.ac.in/nicee/wcee/article/13_1209.pdf.

12. Mazzolani, F. M., G. Della Corte, and M. D'Aniello. 2009. "Experimental Analysis of Steel Dissipative Bracing Systems for Seismic Upgrading." *Journal of Civil Engineering and Management* 15 (1): 7–19. https://doi.org/10.3846/1392-3730.2009.15.7-19.

13. Sarno, L. D., and G. Manfredi. 2010. "Seismic Retrofitting with Buckling Restrained Braces: Application to an Existing Non-ductile RC Framed Building." *Soil Dynamics and Earthquake Engineering* 30 (11): 1279–1297. https://doi.org/10.1016/j.soildyn.2010.06.001.

14. Oviedo A., J. A., M. Midorikawa, and T. Asari. 2010. "Earthquake Response of Ten-Story Story-Drift-Controlled Reinforced Concrete Frames with Hysteretic Dampers." *Engineering Structures* 32: 1735–1746. https://doi.org/10.1016/j.engstruct.2010.02.025.

15. Guerrero, H, T. Ji, J. A. Escobar, and A. Teran-Gilmore. 2018. "Effects of Buckling-Restrained Braces on Reinforced Concrete Precast Models Subjected to Shaking Table Excitation." *Engineering Structures* 163: 294–310. https://doi.org/10.1016/j.engstruct.2018.02.055.

16. Viano, J. D., and T. C. Schaeffer. 2017. "Novel Use of Buckling-Restrained Braces in Precast Concrete Frames." *PCI Journal* 62 (5): 28–34. https://doi.org/10.15554/pcij62.5-03.

17. Mazzoni, S., F. McKenna, M. H. Scott, and G. L. Fenves. 2006. *OpenSees Command Language Manual*. Berkeley, CA: Pacific Earthquake Engineering Research Center, University of California, Berkeley. https://opensees.berkeley.edu/OpenSees/manuals/usermanual/OpenSeesCommandLanguageManualJune2006.pdf.

18. Prakash, V., G. Powell, and S. D. Campbell. 1993. *DRAIN-2DX Base Program Description and User Guide; Version 1.10*. Report UCB/SEMM-93/17. Berkeley, CA: Structural Engineering Mechanics and Materials, Department of Civil Engineering, University of California, Berkeley. https://nisee.berkeley.edu/elibrary/getpkg?id=DRAIN2DX.

19. FEMA (Federal Emergency Management Agency). 2009. *Quantification of Building Seismic Performance Factors*. FEMA P695. Washington, DC: FEMA.

20. ASCE and SEI. 2016. *Minimum Design Loads and Associated Criteria for Buildings and Other Structures*. ASCE/SEI 7-16. Reston, VA: ASCE. https://doi.org/10.1061/9780784414248.

21. Kersting, R. A., L. A. Fahnestock, and W. A. Lopez. 2015. *Seismic Design of Steel Buckling-Restrained Braced Frames: A Guide for Practicing Engineers*. NEHRP (National Earthquake Hazards Reduction Program) seismic design technical brief 11. Gaithersburg, MD: National Institute of Standards and Technology. https://doi.org/10.6028/NIST.GCR.15-917-34.

22. AISC. 2018. *Seismic Design Manual*. 3rd ed. Chicago, IL: AISC.

23. ACI (American Concrete Institute) Committee 318. 2019. *Building Code Requirements for Structural Concrete (ACI 318-19) and Commentary (ACI 318R-19)*. Farmington Hills, MI: ACI.

24. ANSI (American National Standards Institute) and AISC. 2016. *Specification for Structural Steel Buildings*. ANSI/AISC 360-16. Chicago, IL: AISC.

25. ANSI and AISC. 2016. *Seismic Provisions for Structural Steel Buildings*. ANSI/AISC 341-16. Chicago, IL: AISC.

26. SEAOC. 2013. *Examples for Steel-Framed Buildings*. Vol. 4 of *2012 IBC SEAOC Structural/Seismic Design Manual*. Sacramento, CA: SEAOC.

27. Paulay, T., and M. J. N. Priestley. 1992. *Seismic Design of Reinforced Concrete and Masonry Buildings*. New York, NY: John Wiley & Sons.

28. Aragon, T. A., Y. C. Kurama, and D. F. Meinheit. 2020. "Behavior of Ductile Short-Grouted Seismic Reinforcing Bar-to-Foundation Connections under Adverse Construction Conditions." *PCI Journal* 65 (4): 33–50. https://doi.org/10.15554/pcij65.4-01.

29. Brown, J., and S. Kunnath. 2004. "Low-Cycle Fatigue Failure of Reinforcing Steel Bars." *ACI Materials Journal* 101 (6): 457–466.

30. Kunnath, S., Y. Heo, and J. Mohle. 2009. "Nonlinear Uniaxial Material Model for Reinforcing Steel Bars." *Journal of Structural Engineering* 135 (4): 335–343. https://doi.org/10.1061/(ASCE)0733-9445(2009)135:4(335).

31. Mander, J., F. Panthaki, and A. Kasalanati. 1994. "Low-Cycle Fatigue Behavior of Reinforcing Steel." *Journal of Materials in Civil Engineering* 6 (4): 453–468. https://doi.org/10.1061/(ASCE)0899-1561(1994)6:4(453).

32. Mander, J., M. J. N. Priestley, and R. Park. 1988. "Theoretical Stress-Strain Model for Confined Concrete." *Journal of Structural Engineering* 114 (8): 1804–1826. https://doi.org/10.1061/(ASCE)0733-9445(1988)114:8(1804).

33. Coleman, J., and E. Spacone. 2001. "Localization Issues in Force-Based Frame Elements." *Journal of Structural Engineering* 127 (11): 1257–1266. https://doi.org/10.1061/(ASCE)0733-9445(2001)127:11(1257).

34. Pugh, J. S., L. N. Lowes, and D. E. Lehman. 2015. "Nonlinear Line-Element Modeling of Flexural Reinforced Concrete Walls." *Engineering Structures* 104: 174–192. https://doi.org/10.1016/j.engstruct.2015.08.037.

35. Vásquez, J. A., J. C. De la Llera, and M. A. Hube. 2016. "A Regularized Fiber Element Model for Reinforced Concrete Shear Walls." *Earthquake Engineering and Structural Dynamics* 45 (13): 2063–2083. https://doi.org/10.1002/eqe.2731.

36. Pozo, J. D., M. A. Hube, and Y. C. Kurama. 2021. "Effect of Material Regularization in Plastic Hinge Integration Analysis of Slender Planar RC Walls." *Engineering Structures* 239 (15): 112302. https://doi.org/10.1016/j.engstruct.2021.112302.

37. Corley, W. G. 1966. "Rotational Capacity of Reinforced Concrete Beams." *Journal of the Structural Division* 92 (5): 121–146. https://doi.org/10.1061/JSDEAG.0001504.

38. Mattock, A. H. 1967. "Rotational Capacity of Hinging Regions in Reinforced Concrete Beams." *Journal of the Structural Division* 93 (2): 519–522.

39. Priestley, M. J. N., and R. Park. 1987. "Strength and Ductility of Concrete Bridge Columns under Seismic Loading." *ACI Structural Journal* 84 (1): 61–76.

40. Berry, M. P., D. E. Lehman, and L. N. Lowes. 2008. "Lumped-Plasticity Model for Performance Simulation of Bridge Columns." *ACI Structural Journal* 105 (3): 270–279.

41. Ameli, M. J., and C. P. Pantelides. 2016. "Seismic Analysis of Precast Concrete Bridge Columns Connected with Grouted Splice Sleeve Connectors." *Journal of Structural Engineering* 143 (2). https://doi.org/10.1061/(ASCE)ST.1943-541X.0001678.

42. Saxey, B., Z. Vidmar, C.-H. Li, M. Reynolds, and C.-M. Uang. 2020. "A Predictive Low-Cycle Fatigue Model for Buckling Restrained Braces." 17th World Conference on Earthquake Engineering, Sendai, Japan 2020/21.

43. Bruneau, M., E. Kizilarslan, A. H. Varma, M. Broberg, S. Shafaei, and J. Seo. 2019. *R-Factors for Coupled Composite Plate Shear Walls/Concrete Filled (CC-PSW/CF)*. AISC report CPF#05-17. https://www.aisc.org/technical-resources/research/researchlibrary/r-factors-for-coupled-composite-plate-shear-walls--concrete-filled-cc-pswcf.

44. Tauberg N. A., K. Kolozvari, and J. W. Wallace. 2019. *Ductile Reinforced Concrete Coupled Walls: FEMA P695 Study*. Los Angeles, CA: Department of Civil and Environmental Engineering, University of California, Los Angeles. https://www.concrete.org/publications/internationalconcreteabstractsportal.aspx?m=details&i=51722462.

45. Vamvatsikos, D., and C. A. Cornell. 2002. "Incremental Dynamic Analysis." *Earthquake Engineering and Structural Dynamics* 31 (3): 491–514. https://doi.org/10.1002/eqe.141.

46. PEER (Pacific Earthquake Engineering Research Center). 2006. *PEER NGA Database*. Berkeley: PEER, University of California, Berkeley. https://ngawest2.berkeley.edu.

Notation

A_g = gross area of beam or column section, neglecting reinforcement

A_{sc} = steel core (yielding) area of brace

$A_{sc,min}$ = minimum steel core (yielding) area of brace

A_{st} = total area of longitudinal reinforcement in beam or column section

B_I = numerical coefficient for effective damping

BRB_C = adjusted brace force in compression

BRB_T = adjusted brace force in tension

C_d = deflection amplification factor

C_u = coefficient for upper limit on calculated period

d = distance from extreme compression fiber to centroid of longitudinal tension reinforcement

d_b = nominal diameter of longitudinal reinforcing bar

D = average distributed dead load

E_c = initial concrete stiffness

f_c' = specified (design) compressive strength of concrete

f_{sy} = specified (design) yield strength of reinforcing steel

f_{ymax} = highest expected steel core yield strength of brace

f_{ymin} = lowest expected steel core yield strength of brace

F_y = net upward force on beam due to adjusted brace forces in chevron configuration

g = gravitational acceleration

h = depth of beam or column section

I_e = seismic importance factor

I_g = gross moment of inertia of beam or column section, neglecting reinforcement

L = live load

L_p = plastic hinge length

M_u = factored design moment of beam or column

n_b = number of braces in story being designed

N_{QE} = brace axial force under equivalent lateral forces

N_u = factored design brace axial force

P_o = nominal compression (uniaxial) strength of beam or column at zero eccentricity

P_u = factored design axial force of beam or column (positive for compression and negative for tension)

R = response modification coefficient

R_y = adjustment factor for expected brace yield strength

S_{D1} = design spectral response acceleration parameter at 1-second period

S_{DS} = design spectral response acceleration parameter at short periods

S_{MT} = maximum considered earthquake intensity

$\hat{S}_{CT}$ = median collapse intensity

T = fundamental period

T_a = approximate fundamental period

V_{ELF} = design base shear force

V_{max} = maximum base shear strength

V_{story} = shear force in story being designed

z = distance from critical section of beam or column to point of contraflexure

α = angle of brace relative to horizontal

β = adjustment factor for brace force in compression

β_{DR} = uncertainty in design requirements

β_I = effective damping due to inherent dissipation of energy by structure, at or just below effective yield displacement of seismic-force-resisting system

β_{MDL} = modeling uncertainty

β_{RTR} = record-to-record variability

β_{TD} = test data uncertainty

β_{TOT} = total system collapse uncertainty

δ_{DBE} = maximum dynamic roof drift demand at design earthquake intensity

δ_{ELF} = roof drift of effective linear-elastic drift model under equivalent lateral forces

δ_u = ultimate roof drift

$\delta_{y,eff}$ = effective yield roof drift

Δ_{by} = yield deformation of brace

Δ_{max} = maximum brace deformation

$\Delta_{inelastic}$ = inelastic brace deformation

θ = nonlinear story drift

θ_e = effective linear-elastic story drift

μ_c = maximum cumulative inelastic ductility of brace

μ_{max} = maximum ductility of brace

μ_T = period-based ductility of braced frame

ϱ = redundancy factor

ΣM_{nb} = sum of nominal moment strengths of beams framing into joint

ΣM_{nc} = sum of nominal moment strengths of columns framing into joint

ϕ = capacity reduction factor

ω = strain hardening adjustment factor

Ω_0 = system overstrength factor

About the authors

Shane Oh is a PhD candidate in the Department of Civil and Environmental Engineering and Earth Sciences at the University of Notre Dame in Notre Dame, Ind.

Yahya C. Kurama, PhD, PE, is a professor in the Department of Civil and Environmental Engineering and Earth Sciences at the University of Notre Dame.

Jon Mohle, SE, is a senior product and market manager at Clark Pacific in Sacramento, Calif.

Brandt W. Saxey, SE, is technical director at CoreBrace LLC in Salt Lake City, Utah.

Abstract

This paper describes a numerical evaluation of the seismic design of precast concrete buckling-restrained braced frames based on the Federal Emergency Management Agency's *Quantification of Building Seismic Performance Factors* (FEMA P695) methodology. A set of 32 archetype braced frames covering a range of parameters were designed using a procedure consistent with current U.S. building code requirements. Nonlinear numerical models were developed and verified against existing experimental data. The results show that large axial compression and tension forces develop in both beams and columns, thus requiring these members to be designed with large reinforcement ratios or higher-grade reinforcing bars and beams to be designed like column members. Recommended beam and column effective (cracked) linear-elastic axial and flexural stiffness reduction factors provide reasonable estimates of story drifts and brace deformations under design lateral forces. Nonlinear monotonic static pushover and incremental dynamic analyses of the archetypes support an overstrength factor of 2.5, response modification coefficient of 8, and deflection amplification factor of 8 for the seismic design of this system.

https://doi.org/10.15554/pcij66.5-03

Keywords

Buckling-restrained braced frame, deflection amplification factor, FEMA P695, incremental dynamic analysis, monotonic static pushover analysis, precast concrete frame lateral system, response modification coefficient, seismic design, seismic performance factor, system overstrength factor.

Review policy

This paper was reviewed in accordance with the Precast/Prestressed Concrete Institute's peer-review process.

Reader comments

Please address any reader comments to *PCI Journal* editor-in-chief Tom Klemens at tklemens@pci.org or Precast/Prestressed Concrete Institute, c/o *PCI Journal*, 8770 W. Bryn Mawr Ave., Suite 1150, Chicago, IL 60631.